UNIVERSITÀ DEGLI STUDI DI PADOVA

Dipartimento di Fisica e Astronomia "Galileo Galilei"

Master Degree in Physics

Lifetimes measurement in the $f_{7/2}$ shell using the AGATA spectrometer

Thesis supervisor

Dr. Francesco Recchia

Thesis co-supervisor

Rafael Escudeiro

Candidate

Julgen Pellumaj

Academic Year 2019/20

Abstract

The collectivity of the nuclei in the $1f_{7/2}$ shell and the features of their nuclear structure have been extensively studied in the past decades. Investigating the origin of collectivity by using the available spectroscopic data improved the shell model calculations, now able to reproduce the experimental data for the nuclei in this range.

Transition probabilities are essential on understanding the collectivity. Such information can be extracted from precise lifetime measurements of the nuclear excited states. In this thesis the lifetimes of different excited states of the cross conjugate pair of nuclei ^{46}Ti and ^{50}Cr have been measured by using the Doppler Shift Attenuation Method (DSAM). High spin states of these two nuclei have been populated by the fusion-evaporation reaction ^{16}O(^{36}Ar, αn). The experiment was performed in Ganil laboratory on 2018. A beam of ^{36}Ar with energy 115 MeV and intensity 5 pnA was sent in a target which consisted on a thin foil of CaO (550 μg/cm^2 thick) with a gold backing of 10 mg/cm^2 to stop the recoiling nuclei. The advanced gamma-ray spectrometer AGATA has been placed in the close configuration in backward direction with respect to the beam line, to detect the γ-rays emitted from the de-excitation of the products of the reaction. Since many reaction channels are open in a fusion-evaporation reaction, AGATA array has been coupled to NEDA and Neutron Wall (neutron detector array) and Diamant (charged particle detector array) to obtain the needed channel selectivity event by event.

The transition probabilities have been obtained from the experimental lifetimes and compared with literature data and with the results obtained from shell model calculations using the KB3G and the GXPF1A interaction. Rotational collectivity decreasing by the yrast termination of the band has been confirmed in both nuclei.

Contents

List of Tables

List of Figures

Chapter 1

Introductions

Excited nuclear states commonly decay by emission of gamma radiation. This makes the gamma spectroscopy the tool of choice for investigating nuclear structure properties. Different quantities can be measured by gamma spectroscopy, one of them is the lifetime of the level which is inversely proportional to the transition probability. Obtaining this quantity from precise measurements of the lifetime and comparing with the results obtained from calculations based on nuclear shell model, bring fundamental understanding for the nuclear structure. In this chapter a theoretical background is covered and a brief explanation for the working principle of gamma ray tracking array AGATA is given.

1.1 Shell model

The nucleus is a system made of A interactive nucleons, N neutrons and Z protons. To study this system the Schrödinger equation has to be solved.

$$H\psi(r_1, r2, ..., r_A) = E\psi(r_1, r2, ..., r_A) \tag{1.1}$$

where ψ is the wave function which characterize the nuclear state, E its energy and H the Hamiltonian operator. Solving this many body problem it is challenging from the mathematical point of view as a consequence of the nature of the nuclear force itself. The nucleons interact not only through mutual two-body forces but also through three-body

forces as well. Nuclear models are constructed to allow simpler mathematically solvable problems rich in physics, able to reproduce the known properties and to predict others.

Experimental evidences of the existence of the nuclear shells are abundant and were first put forward by Maria Goeppert Mayer [1] and Hans Jensen [2] who in 1949 developed the shell model with nucleons distributed in shells with different energy levels. The measured proton and neutron separation energy showed some similarities with the atomic ionization energy. Some sharp drops occur at the same proton and neutron numbers. These sharp drops discontinuities in the separation energy correspond to the filling of major shells like in the atomic case of the noble gases. These sharp drops were noticed in the so called "magic numbers" *(Z or N = 2, 8, 20, 28, 50, 82, 126)*.

The shell model of nuclei is studied in analogy with the atomic model but in this case the nucleons are assumed to be in the presence of a potential *(nuclear potential)* created from the nucleons itself. This model succeed to reproduce not only the magic numbers but also other properties like the spin and the parity. The nucleons can be considered being in a Wood-Saxon potential (See equation 1.2),

$$V_{ws}(r) = \frac{-V_0}{1 + exp[(r - R)/a]} \tag{1.2}$$

where a $\approx$ 0.5 fm, V_0 is adjusted in 50 MeV in order to give the proper separation energy.

Considering the Hamiltonian of the system as given below in the equation 1.3

$$H = -\frac{\hbar^2}{2m}\nabla^2 + V_{ws} + V_{so} + V_c \tag{1.3}$$

where the V_c is the Coulomb potential, V_{ws} the Wood-Saxon potential and the V_{so} the spin orbit term, the degeneracy of the energy levels break and the shell model reproduce properly the magic numbers [3].

1.2 Collective behaviour of the nucleus

The shell model considers the nucleus as a perfect spherical body without any deformation and its properties depends only on the motion of the valence nucleons. While this kind of

simple model is successful in reproducing the structure of the nuclei near shell closures, it seems to be a very strong assumption when we deal with nuclei in the middle of a shell. In such case many nucleons are contributing to the nuclear state. This may be explained by the collective model of the nucleus.

Considering the rotation and the vibration bands it is possible to reproduce the lower excitation energy of the nuclei in the middle shell. These structures can be properly reproduced by shell model calculations provided a large enough model space in order to allow for coherent contribution from many nucleons.

Rotational band

A nucleus with a non zero quadrupole moment *(nucleon density distribution is not spherically symmetric)* can have excited energy levels because of the rotation of it perpendicular to the axis of symmetry. These states have energies:

$$E = \frac{J(J+1)\hbar}{2I} \tag{1.4}$$

where J is the total angular momentum and the I is the moment of inertia of the nucleus with respect to the rotating axis. The energy levels in the rotational band are proportional with the $J(J+1)$. The energy levels of the nuclei in the middle of the $1f_{7/2}$ shell show a rotor like behaviour.

Vibration band

When the deformation of a nucleus oscillates about its mean value these are called vibration modes. There are different modes of vibration, the lowest and in most cases the most relevant one is the quadrupole vibration. The small oscillations about the equilibrium shape perform simple harmonic motion and the energy of different vibration bands are equidistantly spread from each other. The observation of energy levels equally spaced from each other is interpreted as such shape oscillations.

1.3 Previous studies of the nuclei in the $1f_{7/2}$ shell

Some very interesting features appear to the nuclei in the $1f_{7/2}$ shell like shape co-existence, collective and singe particle behaviour, backbending. These features motivated theoretical and experimental research work in the past years to these nuclei in order to understand their structure. Typically these nuclei show a large prolate deformation in the low energy excited states which decrease as soon at high angular momentum and in particular toward the band termination. The experimental investigation of such phenomenon has been carried out in this thesis. On top of excitation energy, the transition probabilities obtained from precise measurements are essential for understanding this behaviour which have been extensively studied in the past [4]. In the Figure 1.1 is shown a theoretical calculation of the B(E2) values for the nucleus of ^{50}Cr based on the shell model. The calculations predict high B(E2) values in low excited states, translated into high collectivity and short lifetimes of the excited energy levels [5].

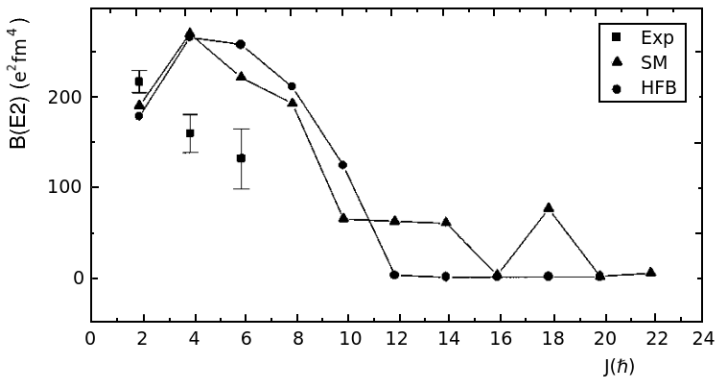

Figure 1.1: B(E2, J→J-2) transition probabilities versus J computed for ^{50}Cr based on the Shell model (SM)-triangles and Hartree Fock Bogoliubov theory(HFB)-circles, compared to the experimental data (exp)-squares. Taken from [6]

To investigate the rotational collectivity the attention is focused on the yrast of the levels up to the band termination in the $1f_{7/2}$ shell. This was very challenging in previous studies since in this mass region the population toward high spin states has low cross sections. The compound nucleus loses significant energy and angular momentum through the evaporation of the particles. The development of large γ-ray detector arrays, like GASP [7] used in these kind of studies in [8][9], with a high detection sensitivity and also the development of high efficiency particle detectors helped on extending the level

schemes in high spin states of the nuclei of interest. In the study reported in this thesis, for the first time the-state-of-art of gamma spectroscopy AGATA has been used for this kind of studies in this experiment.

From the nuclei in the $1f_{7/2}$ shell *(the nuclei between ^{40}Ca and ^{56}Ni)* the ones from the middle and the second part of this region have been extensively studied, especially the ^{48}Cr which has the maximum number of the valence nucleons and shows the highest deformation. ^{46}Ti and ^{50}Cr are the nuclei of our interest in this thesis. In previous studies the reactions used to populate high spin states of the nuclei of ^{46}Ti and ^{50}Cr were (^{28}Si + ^{28}Si) [5][9][10]. ^{24}Mg(^{28}Si,α2p)^{46}Ti [8][11], ^{12}C(^{46}Ti,2α)^{50}Cr [12].

With the spectroscopic data also the theoretical calculations improved in this mass region. The shell model calculations we are able to perform now days for these nuclei have a very good quality. The excitation energies and the transition probabilities are properly reproduced.

1.4 Gamma-ray detection

For energies ranging from a few keV to a few MeV gamma-rays interact with matter through one of the three principal mechanisms: Photoelectric effect *(interaction of the gamma photon with an electron, the energy is totally absorbed resulting on an ionised atom in the medium)*, Compton effect *(elastic collision of a photon with an electron of the medium, the initial energy of the γ-ray is shared between the electron and a scattered γ-ray lower in energy)*, electron-positron pair production *(γ-rays with energy higher than 1022 keV may create $e^- - e^+$ pairs which after annihilation it result in the emission of two 511 keV photons in opposite directions)*.

Depending on the energy of the gamma photon and the characteristics of the material one of these processes is most likely to appear. Below in the Figure 1.2 is shown the probability of each of these processes to take place in the germanium crystal as a function of the energy of the photon. For gamma rays in the energy range from hundreds of keV to a few MeV the Compton scattering process is the dominant interaction mechanism. The gamma rays emitted from the de-excitation of the nucleus are typically in this energy

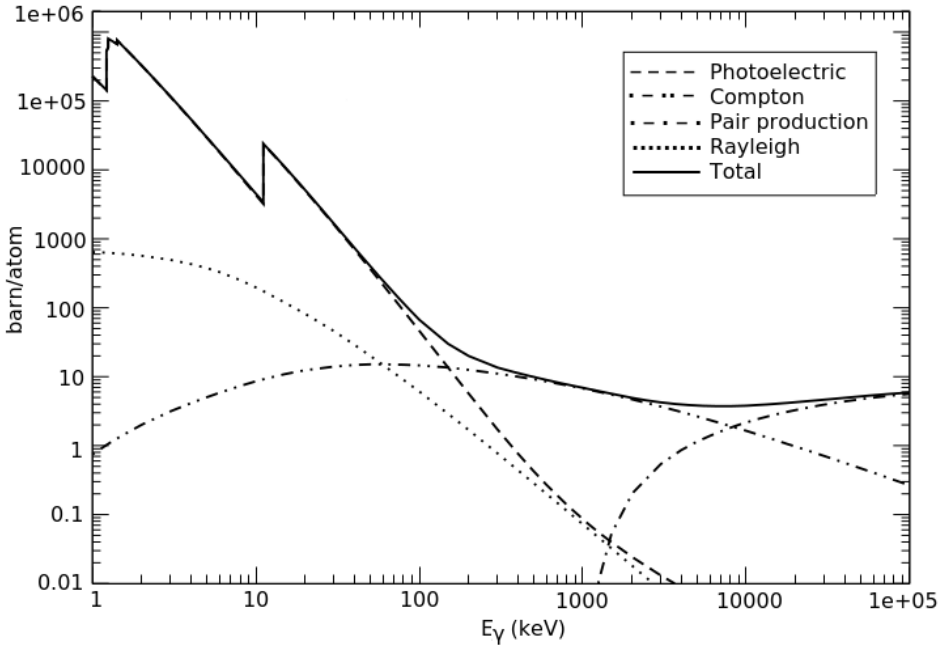

Figure 1.2: The probability of each interaction mechanism of gamma photons in an energy range from 1 keV to 10 MeV, with germanium. Taken from [13]

range.

For the detection of the gamma rays scintillation inorganic crystals has been commonly used till the end of 60s when the lithium-germanium detector (GeLi) was designed. This detector provided a very good energy resolution *(around 2 keV for $E_\gamma \sim$ 1000 keV)* but the efficiency of the early designs was often much lower than the one from scintillation detectors. The development of high resolution γ-ray detectors expanded the limits of what can be observed and has been very important in the study of the nuclear structure.

A major problem of the early designs of germanium detector arrays was the poor peak-to-background ratio *(P/T - the ratio of the number of counts in the photopeak(s) to the total number of counts in the spectrum)* in the spectrum caused by the incomplete energy collection due to the size of the crystal. Early designs had a P/T $\approx$ 25% and the rest of the events was contributing on a continuous background extending to lower energies from the real value of the γ-ray photon energy. This problem was then solved by using the so called "anti-Compton shield" consisting on a second surrounding detector to detect the scattered photons. The events measured in coincidence between the germanium and the shield detector would be rejected. Most commonly used materials in the anti-Compton

shield is BGO, a high dense and high efficiency scintillator material. The anti-Compton shield improved a lot the P/T factor. Below in the Figure 1.3 is shown how the Compton shield influenced the level of the background in the spectrum. The spectrum of ^{60}Co source was obtained with and without the Compton shield.

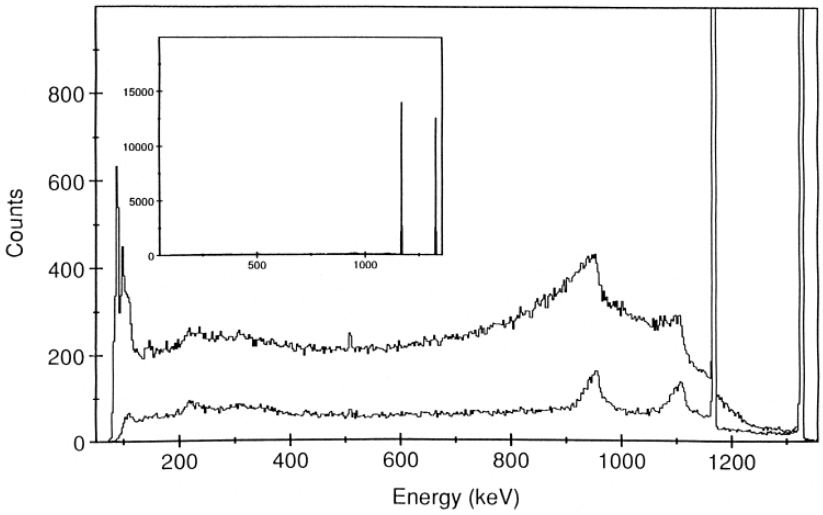

Figure 1.3: The gamma spectrum of ^{60}Co source obtained with and without the anti-Compton shielding around the germanium detectors. Taken from [14]

Around 1990s arrays of Compton-shielded large-volume HPGe detectors -EUROGAM [15], EUROBALL [16] and GAMMASPHERE [17] were constructed. This brought a big evolution in the gamma spectroscopy. Lately even more powerful detectors namely "tracking detectors" were developed like GRETA [18] in US and AGATA [19] in Europe.

1.5 Principle of gamma ray tracking array

The energy of the gamma rays is released in a discrete number of interactions. The purpose of the gamma ray tracking detectors is to reconstruct the path that the scattered gamma photons follow inside the detector based on the position and energy deposit in each interaction. For every event the energies, the incident and the scattering directions should be measured. Those events which partially deposit their energy in the detector should be rejected. In order to be able to perform such measurements one should know the interaction position and the energy. Compton scattering is the main interaction mechanism of gamma photons with energy from 100 keV to 10 MeV with the atoms of

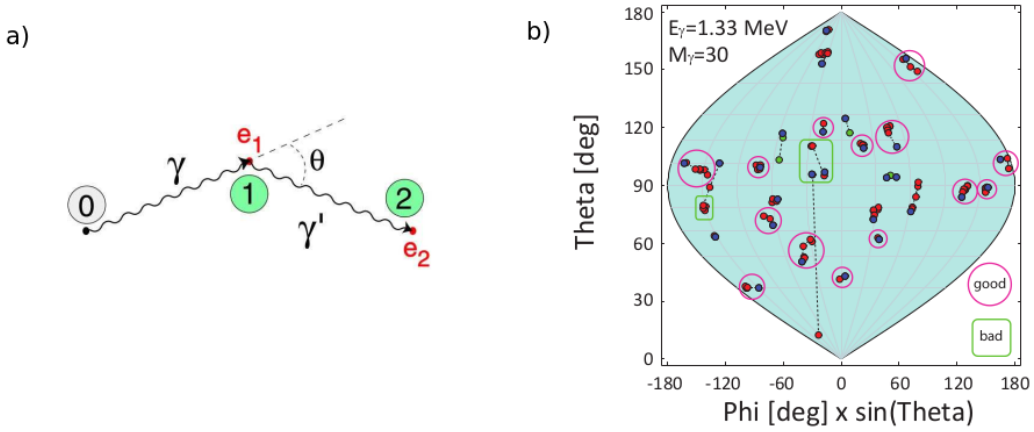

Figure 1.4: a) Example of gamma ray tracking after a Compton scattering before being photo-absorbed. b) Representation of 30 gamma events with energy E_γ=1MeV detected in the ideal germanium shell and reconstructed with the clustering technique. [14]

a germanium detector. (See Figure 1.2). Based on the Compton formula (Eqn.1.5), it is possible to track the path of a gamma ray inside the detector. E'_γ it refers to the energy of the scattered gamma photon, E_γ it refers to the initial energy and θ to the scattering angle.

$$E'_\gamma = \frac{E_\gamma}{1 + \frac{E_\gamma}{m_0 c^2}(1 - cos\theta)} \tag{1.5}$$

Let's suppose a γ-ray photon with energy E_γ is entering in the germanium detector, it is scattered in the position 1 by an electron and then the scattered gamma photon with energy E'_γ is absorbed by another interaction in the position 2. (See Figure 1.4.a)

In the position 1 where the Compton scattering take place, the detector measure the energy of the electron "e_1". Knowing the direction from which the incident gamma-ray is coming and the energy of the electron, with the help of equation 1.5 is possible to get the energy of the scattered gamma-ray, $E'_\gamma = E_\gamma - e_1$. This energy is going to be equal with the energy of the electron measured from the detector on the position 2 "e_2". The measured value of energy is going to be compared with the one obtained from the algorithms of AGATA based on the principle described above. If the measured energy of an reconstructed event is the same as the one calculated from the tracking algorithms based on the interaction points and scattering angles the event is recorded, otherwise it is rejected.

This calculation it would be necessary to be performed for every possible sequence of interaction but since in case of large gamma multiplicity there is a large number of cases to be computed another technique should be used and that is called the Clustering technique (See Figure 1.4.b). The total absorption length for a gamma photon is on the order of a few centimeters so the interaction position points of one gamma should be localised in a small region of the detector. Based on the angular separation of the interaction points, the interactions which belong the same track can be clustered. The points separated by a smaller then a reference angle θ are classified in the same cluster. Then the validity of the cluster is checked by the Compton scattering formula. (See Eqn.1.5).

There are some limitations on the performance of the tracking algorithms, like for example the interaction position is different from the position of the energy deposition of the electron as a consequence of electron range in material. Electrons can lose energy via Bremsstrahlung and also low energy gammas undergo Rayleight scattering which result in the change of the direction without losing energy.

1.6 AGATA - state-of-art of gamma spectroscopy

Advanced GAmma-ray Tracking Array (AGATA) is a collaboration project of some European countries. This new generation of γ tracking arrays it will be used for high resolution γ-ray spectroscopy of the reaction channels induced by stable and radioactive beams. In the final configuration, as shown in the Figure 1.5.a, AGATA will be a 4π sphere composed of 180 HPGe detectors grouped in triple clusters which runs on fully digital electronics. The inner radius of the sphere is about 30 cm which allow the installation of other detectors inside the array for a channel selection of the reaction. Each cluster is composed of three differently shaped hexagonal tapered coaxial HPGe detectors, encapsulated in a sealed thin aluminum case. The crystals have a length of 90 mm and are electrically divided in 36 segments. A representation of the segmentation of the germanium crystal and its geometry is shown in Figure 1.5.b. The high electrical segmentation of the crystals gives the possibility to track the trajectories of the γ-rays inside the detector. By sophisticated algorithms the energy of the γ-rays is reconstructed and the background is

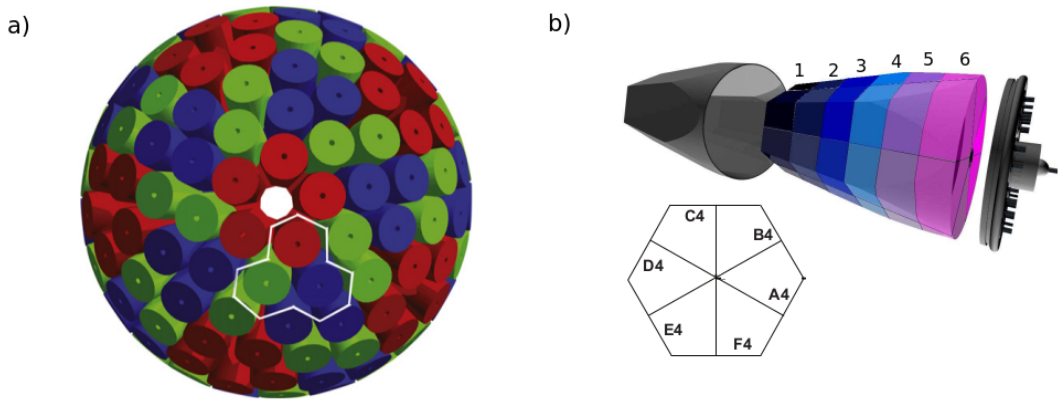

Figure 1.5: a) The final configuration of AGATA b) The geometry of the highly segmented germanium detector. Taken from [20]

reduced by rejecting events which doesn't correspond to realistic Compton scattering as it was mentioned in the previous section. In this way the need for Anti-Compton shielding is avoided allowing a larger fraction of the solid angle to be covered by the detectors.

A good Doppler correction on 'in beam gamma spectroscopy' is of a vital importance in order to measure the proper energies of the γ-rays detected. This can be done by knowing the angle between the emitting nucleus and the γ-ray photon which it is possible with the highly segmented germanium crystals on AGATA and the pulse shape analysis of the signals on them resulting from the interaction of the photon with the medium. When a gamma-ray deposits totally *(photoelectric)* or partially *(Compton)* its energy in one of the segments of the crystal, free electrons or electron-hole pairs respectively for both cases are going to be created and resulting in a net charge collected on the electrodes. Meanwhile in the neighbouring segments a signal is induced (see Figure 1.6). The first interaction point is considered the one with the highest signal, in our case on Figure 1.6 the highest signal is on the B4 segment. Analysing the shape of the signal in this segment and in the neighbouring segments and by comparing them with some reference ones obtained by simulating different electric field on the segments, information which is saved in the AGATA libraries, it is possible to reconstruct the position of interaction with a very good resolution. Once the positions of the interactions are obtained it is possible to use properly tuned algorithm, named tracking algorithms, to follow the path of the gamma-ray inside the detector.

The fine segmentation and large number of detectors of the AGATA array result in a high selectivity and sensitivity superior to other existing γ-ray tracking arrays.

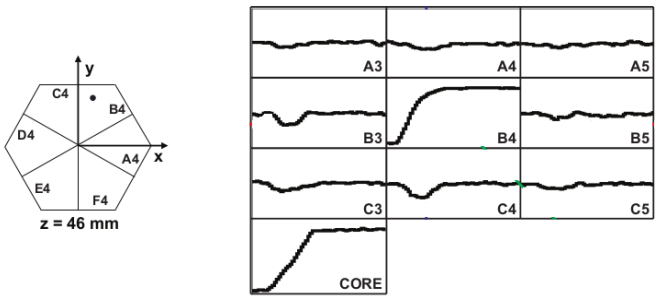

Figure 1.6: Example of the pulse shape analysis of the signals from the segments of the Ge crystal. Taken from [21]

Chapter 2

The experiment and the setup

In this chapter the reaction and the experimental apparatus used to select the reaction channels will be described. A brief summary of different techniques developed for lifetime measurements in different time ranges focusing in the Doppler Shift Attenuation method will be given.

2.1 The experiment

The experiment described in this thesis took place in Ganil laboratory (Caen, France) in 2018 with the purpose of studying the isospin symmetry in mirror pair nuclei. The excited states of the nuclei of interest have been populated by a fusion evaporation reaction ^{16}O(^{36}Ar, αn). A beam of ^{36}Ar with intensity $3 \cdot 10^{10}$ pps and energy 115 MeV was sent to a target which consisted on a thin foil of CaO 550 $\mu g/cm^2$ thick. Right after the target a backing of gold (^{130}Au) with thickness 10 mg/cm^2 was placed. The products of the reaction created in the target will slow down until stopping inside the backing.

For this experiment AGATA was coupled for the first time with two ancillary detectors, NEDA and Neutron Wall*(neutron detector array)* and Diamant *(light charged particle detector array)*, represented in the Figure 2.1. Measuring the gamma rays in coincidence with the particles evaporated from the compound nucleus will help in classifying the collected data into different channels which are open in the reaction. More details about the setup will be given later in this chapter.

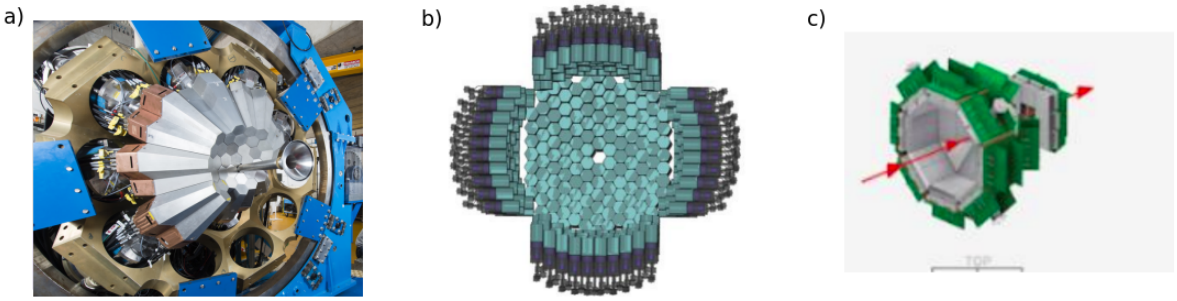

Figure 2.1: The experimental setup a) AGATA, b) NEDA, and c) Diamant

2.2 Fusion-evaporation reactions

Fusion-evaporation reactions are a very good way to produce nuclei in a high spin state as in the case of the light nuclei of interest for this thesis. A beam of a heavy ion is accelerated in an energy of a few MeV/A and is collided with a target nucleus and they fuse together. If the fast fission doesn't occur then a highly excited nucleus called 'compound nucleus'

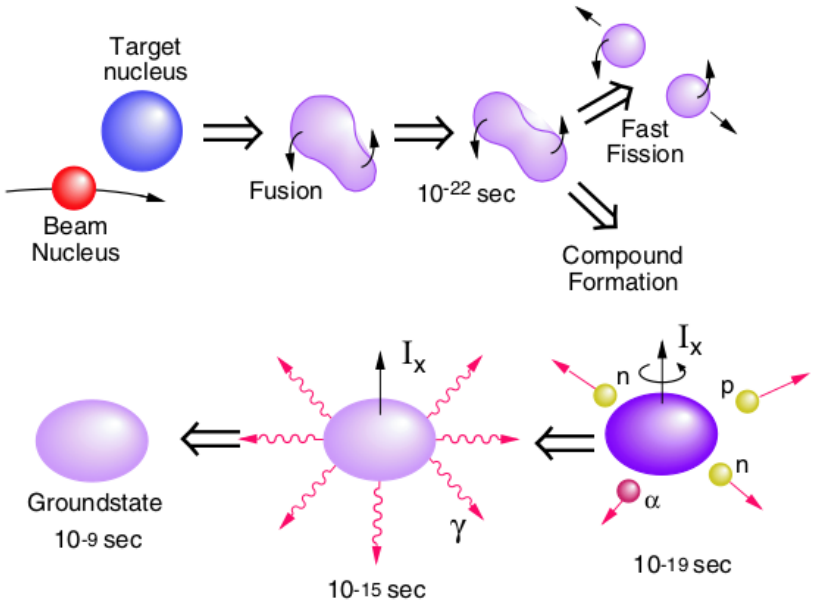

Figure 2.2: Schematic representation of fusion-evaporation reactions. Taken from [22]

is formed. The compound nucleus is charged and rapidly rotating. In a very short time of the order of 10^{-19} seconds after the compound was formed light particles like protons, neutrons, and alphas are evaporated carrying with them energy and angular momentum. After the evaporation of the particles the compound nucleus it is still rotating very fast and in a highly excited state. It loses the rest of the energy and angular momentum by

the emission of gamma rays.

In the Table 2.1 are shown the corresponding cross sections as calculated from the PACE4 software [23] for the channels open on the reaction ^{16}O(^{36}Ar, αn) used to produce the nuclei of interest in the experiment described in this thesis.

Table 2.1: The channels open in the reaction and their corresponding cross sections calculated using the PACE4 software

Z	N	A	Element	X-section (mb)	Channel
24	25	49	Cr	348	1n 2p 0a
24	23	47	Cr	6.19	1n 0p 1a
23	24	47	V	145	0n 1p 1a
21	22	43	Sc	4.36	0n 1p 2a
23	26	49	V	131	0n 3p 0a
24	24	48	Cr	2.67	0n 0p 1a
22	24	46	Ti	82.8	0n 2p 1a
23	25	48	V	1.4	1n 3p 0a
24	26	50	Cr	73.2	0n 2p 0a
25	24	49	Mn	0.93	2n 1p 0a
25	25	50	Mn	45.5	1n 1p 0a
25	26	51	Mn	0.378	0n 1p 0a
22	22	44	Ti	19.9	0n 0p 2a
20	20	40	Ca	0.32	0n 0p 3a
23	23	46	V	10.7	1n 1p 1a
26	24	50	Fe	0.233	2n 0p 0a

We are interested in the study of two nuclei ^{46}Ti and ^{50}Cr, $2p1a$ and $2p$ channel respectively.

$$^{36}Ar + ^{16}O \rightarrow (^{52}Fe)^{*} \rightarrow ^{46}Ti + 2p + \alpha$$

$$^{36}Ar + ^{16}O \rightarrow (^{52}Fe)^{*} \rightarrow ^{50}Cr + 2p$$

2.3 Experimental setup

In this experiment NEDA + Neutron Wall and Diamant were coupled together with AGATA used to identify the reaction channel event by event. In order to measure the lifetime the DSAM technique *(described in chapter 2.5)* was used, based on shape analysis of the peaks recorded from the experiment. A lot of channels are open in a fusion

evaporation reaction and this require the use of ancillary detectors to properly select the reaction channel.

2.3.1 NEDA

The NEutron Detector Array (NEDA) is a neutron detection system designed to operate in conjunction with γ-ray arrays at stable and radioactive beams for nuclear spectroscopy studies. It is used as a neutron tagging instrument and measure neutrons emitted from outgoing channels especially in fusion-evaporation reactions. NEDA is very effective in the study of the nuclei populated by these reactions. It has a very high-detection efficiency for neutrons and very good neutron-γ discrimination capabilities at high counting rates [24].

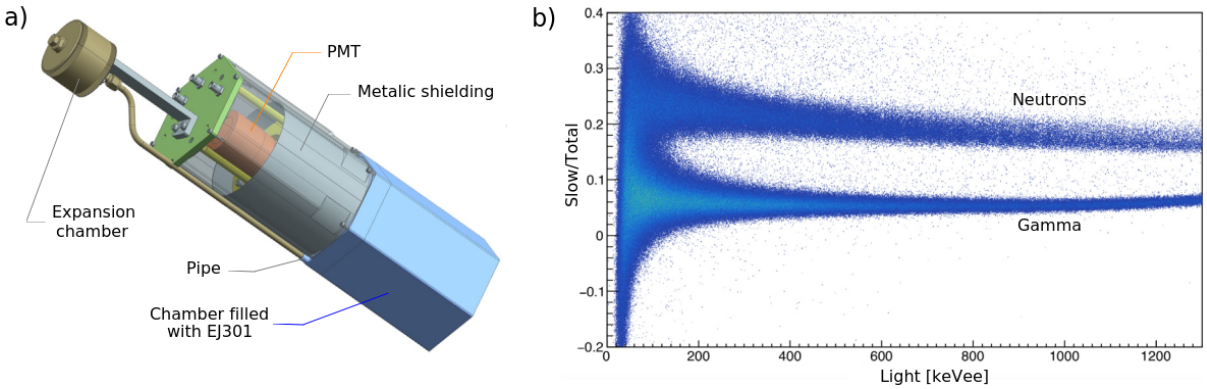

Figure 2.3: a) A NEDA single detector has a hexagonal shape and contains the PMT surrounded by a metallic shielding and a cell filled with liquid scintillator EJ301, this cell is connected with a pipe to an expansion chamber to allow the change in volume of the scintillator with temperature. b) Neutron-gamma discrimination based on the charge comparison method. Taken from [24]

In this experiment NEDA was composed of 95 single detectors located one meter from the target. This configuration allow an improvement of the neutron-γ discrimination based on the Time-of-Flight (ToF) measurements but also the neutron angular distribution. The geometry of NEDA detector array is shown in Figure 2.1.a. A single NEDA detector has the shape of a regular hexagon that allows for a fully tiled up surface. It is build of a photo multiplier tube (PMT) with a length of around 20 cm and the active volume of the detector is filled with liquid organic scintillator Eljen EJ301. (See Figure 2.3.a)

More information for the data recorded from NEDA and the neutron channel selection will be given in the next chapter.

2.3.2 Diamant

For reaching a high selectivity of the reaction channels Diamant has been used in this experiment as a proton and alpha particle tagging instrument. Diamant is a 4π charged particle detector array made of 84 CsI(Ti) coupled to a plexi-glass light guide and to PIN photodiodes. It was developed to serve as an ancillary detector inside large gamma-detector arrays.

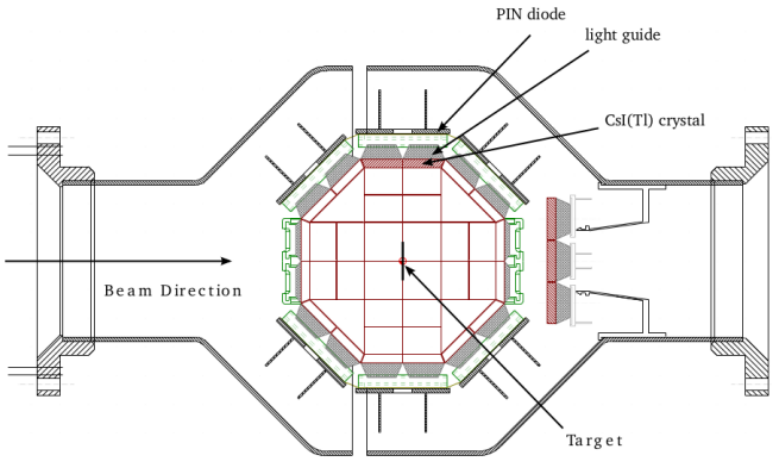

Figure 2.4: A configuration of the Diamant detector array in the experiment. Taken from [25]

Each single detector of Diamant is made of a 3 mm CsI(Ti) scintillation crystal which is commonly used on the charged particle discrimination because of the slow and the fast component of their signal which depend on the type of the particle. Three types of information are extracted from the signals of the detector, the energy, particle type and the time reference. The CsI crystals are shielded from the elastically scattered beam ions by a tantalum absorber foil. This detector has a very good efficiency, a very good discrimination between the protons and alpha particles and also it is partially transparent to gamma-rays.

In the Table 2.2 some characteristics of the Diamant detector array are shown.

Table 2.2: The main characteristics of Diamant. Taken from [20]

Number of CsI crystal detectors	84
Solid angle coverage	90%
Energy resolution at 5.5 MeV	2%
Nominal α efficiency	50%
Nominal proton efficiency	70%

2.3.3 AGATA

AGATA in our experiment was used in the backward configuration. A total of 34 germanium detectors were used, arranged in 12 clusters as represented in the schematic view below (Figure 2.5). The previous use of AGATA has influenced the energy resolution of its germanium detectors, especially the neutron damage of the crystals. The energy resolution at 1000 keV is about 2.5 keV FWHM and at 2000 keV is about 3.5 keV FWHM.

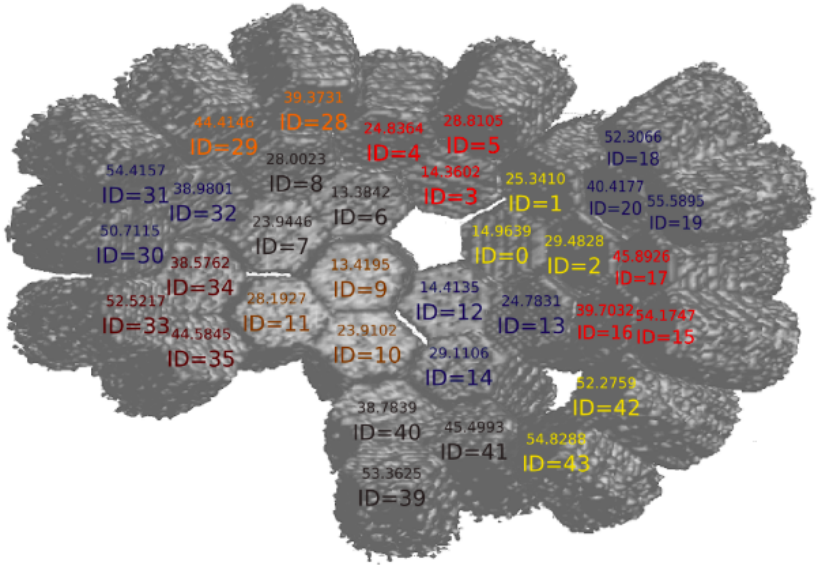

Figure 2.5: The configuration of AGATA in the experiment

The neutron damage of AGATA

In fusion-evaporation reactions the neutrons emitted from the residual nucleus have a Maxwellian distribution with a maximum at energies at a few MeV and due to the kinematics of the reaction they have angular distribution peaked at forward angels with

respect to the beam direction. The germanium crystal is very sensitive to the fast neutrons.

The interaction of the neutrons with the germanium cause some defects on its lattice. These defects are charged and can interact with the charge carriers *(electrons and holes)* inside the detector causing a decrease of the charge collection efficiency. Consequently the gamma peaks in the spectrum appears with a tail on the left side. The n-type crystals are less sensitive to the neutron damage than the p-type. Since the defects are negatively charged the e^- carriers are not trapped as the holes. Because of the different behaviour of electrons and holes the effect of neutron damage depends on the position of the interaction (See Figure 2.6.a). AGATA uses the position to correct the measured energy, obtaining this way a much better resolution. The effect of the correction can be appreciated in the Figure 2.6.b.

The neutron damage influence the left side of the lineshapes where it is expected to see the tails emerging from the lifetime of the nuclear energy levels. This is why the response function of the detectors should be well known and properly implemented in the Monte Carlo simulation code used for the lineshape analysis.

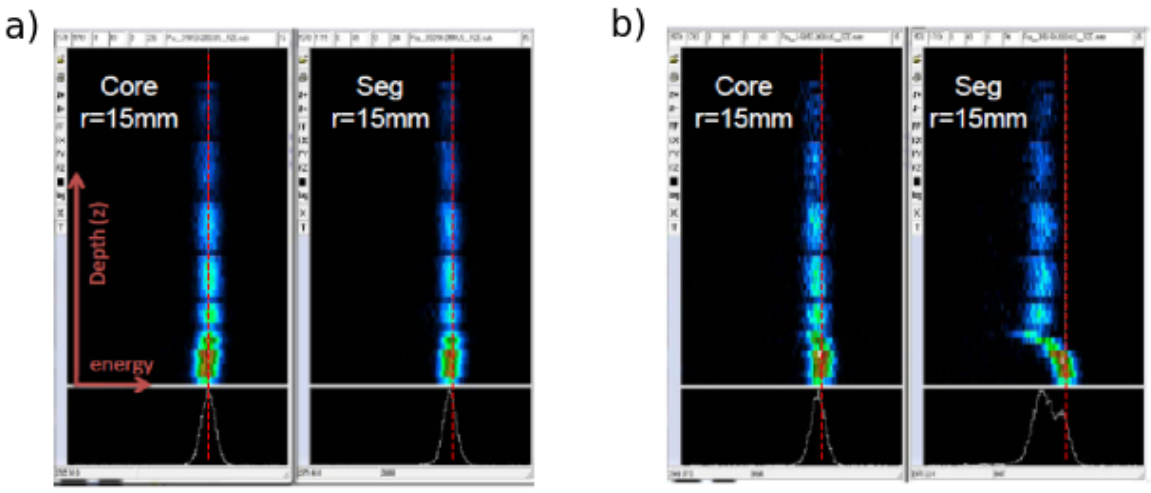

Figure 2.6: The effect of the neutron damage on the energy resolution of the germanium detectors of AGATA. Taken from [21]

2.4 Data collection and processing

AGATA has been coupled with NEDA + Neutron Wall and Diamant, two ancillary detector arrays used as neutron and light charge particle tagging instruments respectively. Coincidence measurements with the detectors of the setup allow a separation of the data collected from the experiment into different channels open in the reaction.

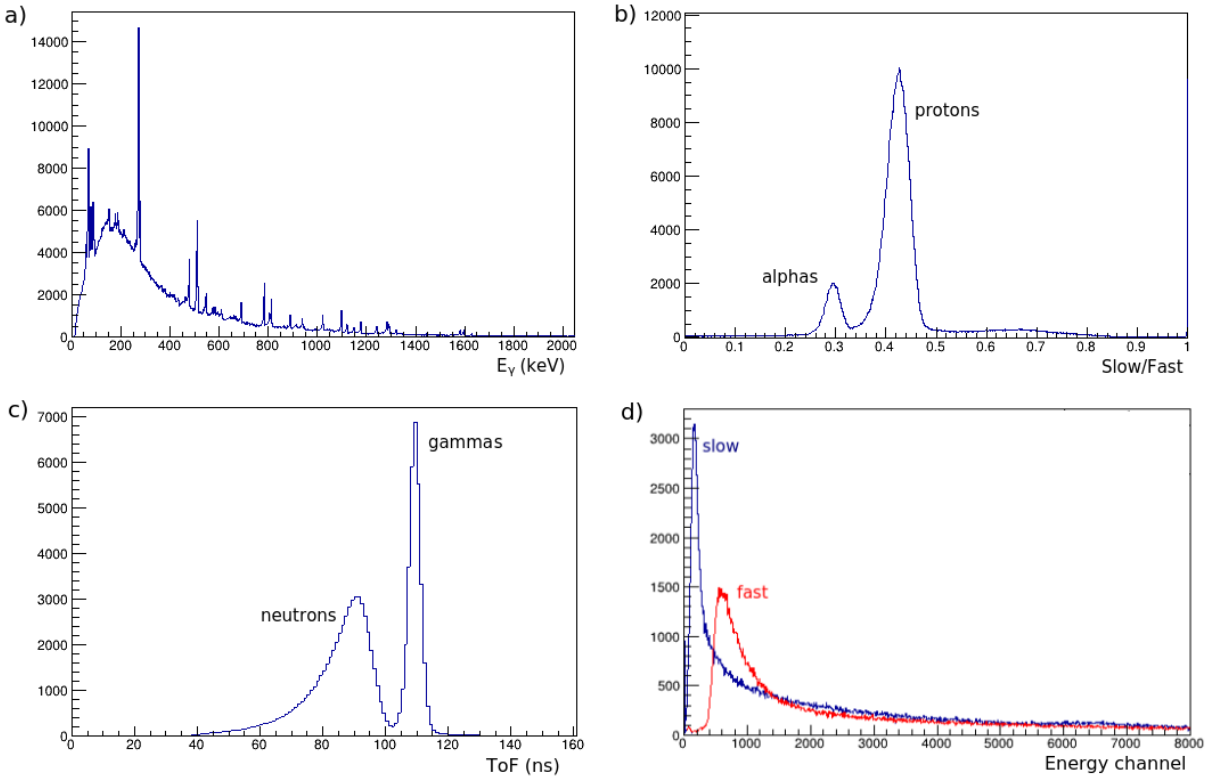

Figure 2.7: a) Gamma ray spectrum obtained from AGATA. b) The ratio between the integral of the slow and the fast component generated from the signal in one of the crystals of Diamant. c) Time of Flight (ToF) obtained from one of the detectors of NEDA, the gamma rays and the neutrons have different time of flights, this can be used for the γ-neutron discrimination. d) The integral of the slow and the fast component generated from the signal in one of the detectors of NEDA.

All the information for the detected events like gamma rays, neutrons and charged particles *(protons and alphas)* is stored in three branches, namely AGATA, NEDA and Diamant respectively. For the gamma-rays detected information like the crystal Id and the segment where the gamma-ray interacts, the global time of the interaction, the position interaction point and the energy are all stored on the AGATA data. For the detected neutrons information like the energy, the integral of the fast and the slow component generated from the signal, the crystal Id where the interaction take place and the global

time stamp are stored. Meanwhile for the protons and alpha particles detected the same information as in the case of the neutrons including the ratio between the integral of the slow and the fast component generated from the detected particle are stored on the data of Diamant. Some of these data are plotted in the Figure 2.7.

All this information is going to be used for the reaction channel selectivity which will be discussed in the next chapter.

2.5 Measurements of nuclear level lifetime

The nuclear level lifetime is another important quantity that one can measure. The lifetimes are proportional to transition probabilities and precise measurements of those can highlight properties of nuclear structure by comparing their values obtained from shell model calculations with the one experimentally estimated from the level lifetime.

2.5.1 Doppler-based methods for lifetime measurement

The lifetime of the excited nuclear levels which decay by gamma emission varies from 10^{-16} to 10^{-3} seconds depending on the strength and the energy of the transition. Different techniques have been developed to measure different ranges of these lifetimes and they are classified in two groups: techniques involved in direct measurement of the time difference between two successive gamma-rays and those which are based on the Doppler shift effects. In the former case there are some limitations because of the rise time of the voltage pulses but with the now days technologies it is possible on reaching lifetime measurements till the order of nanoseconds. In the Figure 2.8 the time range covered by different techniques is given.

Doppler Shift techniques are typically used to measure short lifetimes varying in a range from hundreds of nanoseconds down to a few femtoseconds. From the Doppler Shift based techniques most commonly used are the Recoil Distance Method and DSAM. The Recoil Distance Method technique uses a thin target where the reaction takes place followed from a stopper placed in a certain distance from it. This distance is chosen basing

on the calculations of the kinematics of the reaction and the lifetimes of the energy levels which will be measured. The de-excitation of the nucleus in flight when it is located in between the target and the stopper will cause a shift of the peak in the energy spectrum because of the Doppler shift effect. The gamma-rays emitted from the nucleus inside the stopper will appear unshifted in the energy spectrum. One can obtain the lifetime of the energy level by comparing the intensities of the shifted peak and the unshifted one of the same gamma-ray for different distances between the target and the stopper. This technique is used for measuring lifetimes from a few picoseconds to tens of nanoseconds.

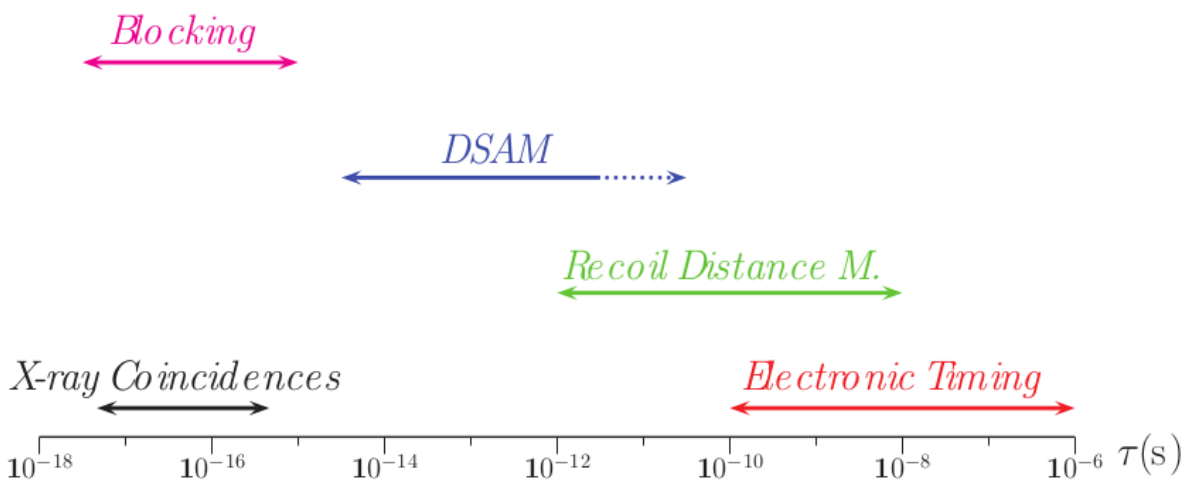

Figure 2.8: The main techniques for lifetime measurements and the time range covered from each of them. Taken from [21]

2.5.2 Doppler Shift Attenuation method

Doppler Shift Attenuation method is a very powerful technique for measuring lifetimes from a few femtoseconds to tens of picoseconds.

This method consist in a very thin target where the reaction takes place and a backing which is placed right after it in order to stop the emitting nuclei produced from the reaction. If the lifetime of the excited energy levels of the nucleus created from the reaction is comparable with the stopping time of it inside the backing, it is possible that the gamma decay of the excited nucleus takes place when it is still slowing down.

When a gamma photon with energy E_γ is emitted by a nucleus moving with a velocity

$\vec{v}$, the gamma-ray energy observed at an angle θ between the recoil and the γ-ray emission direction follows the Doppler relation:

$$E_{\gamma}^{'} = E_{\gamma} \frac{\sqrt{1-\beta^2}}{1-\beta cos\theta} \tag{2.1}$$

where $\beta = v/c$.

From the formula 2.1 it can be understood that the energy of the γ-ray photon, if it is emitted from a nucleus moving with velocity $\vec{v}$, it depends on the angle where it is observed. A smaller energy it is observed in backward angles and bigger in the forward angles. For fusion-evaporation reactions the emitting nuclei travel along the beam. This is a very good approximation for these types of reactions.

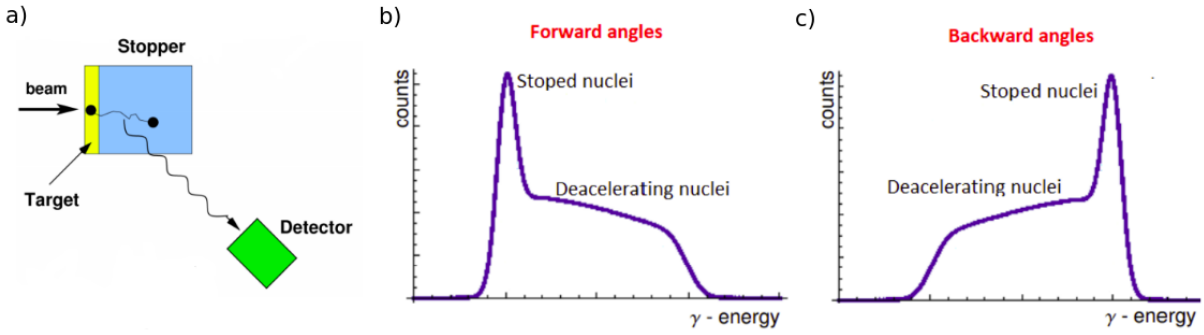

Figure 2.9: a) A schematic view of a) DSAM experiment b) the measured energy spectrum in the forward angles c) the measured energy spectrum in the backward angles

Being the slowing down process continuous and the γ-ray emission statistical, the measured spectrum of the γ-s corresponding to a particular transition is a continuous distribution ranging between the nominal rest energy and the maximum Doppler Shift. The lineshape *(distribution)* depends on the lifetime of the level, on the kinematics of the emitting nuclei, on the slowing down properties of the absorbing medium and also it depends on the angle between the beam line and the detector (See Figure 2.9.b and 2.9.c). In our case AGATA has been used in the backward configurations that is most sensitive for lifetime measurements. Because of the short lifetime of the nuclear energy levels, the lineshapes in the energy spectrum are going to have a deformation *(tail)* on the left side.

As the main sources of uncertainty and limitations of the Doppler Shift Attenuation method we can mention: the kinematics of the nuclei inside the stopper, the side feeding and the limited knowledge for the population of the energy levels from the reaction.

2.5.3 Monte Carlo simulation code

In the DSAM method the lifetimes can be extracted by analysing the shapes of the peaks resulting from the experiment and comparing them with model calculations. A very sophisticated Monte Carlo simulation code [26] developed from the gamma spectroscopy group of University of Padova has been used to obtain a simulated spectrum. The simulated gamma energy spectrum is then compared with the experimental one. The user can change the lifetimes of the energy levels and also their population until a good agreement between the two spectra is achieved and the deformations on the peaks are reproduced.

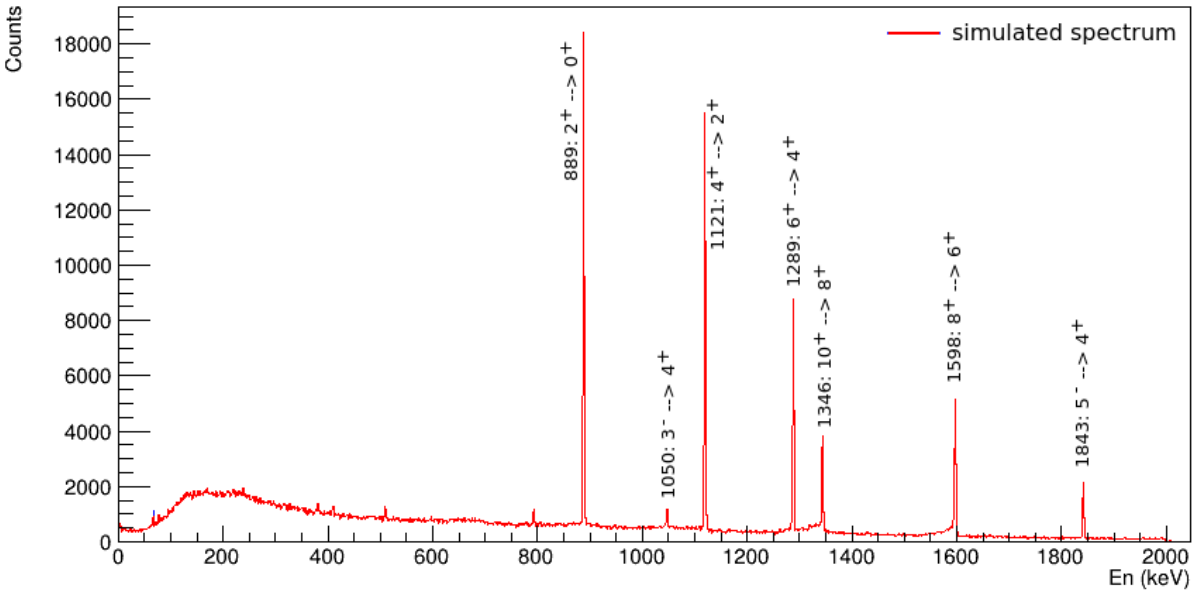

Figure 2.10: A simulated spectrum of ^{46}Ti from the Monte Carlo simulation

In the Figure 2.10 a spectrum obtained from the simulations is represented. This spectrum of ^{46}Ti was obtained by populating some of its energy levels: the 6242 keV, 4897 keV and 3852 keV. The gamma-rays emitted by these energy levels can be observed in the spectrum. The deformed shapes on the left side of some of the peaks *(tails)* observed in the spectrum are a consequence of the energy level lifetime.

This code takes into consideration a lot of conditions of our experiment some of which are listed below:

- The fusion evaporation reaction. The projectile, the target, the residual *(nucleus of interest)* are implemented in the code
- The kinematics of the residual nucleus inside the stopper. This is very important since it is one of the factors which leads into uncertainties on the DSAM
- The gamma decay of the residual nucleus follows complicated level schemes taking in consideration the lifetime of the energy levels
- The response function of the detectors
- The geometry

Chapter 3

Data analysis

^{46}Ti and ^{50}Cr are the nuclei of interest for the present study and two of the strongest populated reaction channels in the experiment. Their level schemes have been reconstructed by analysing the gamma ray spectra obtained from coincidence measurements with the germanium crystals of AGATA. The lifetimes of their energy levels at reach using the DSAM technique were obtained by comparison to the Monte Carlo simulations. The details are presented in this chapter together with the procedure for the channel selection.

3.1 Channel selection

The raw data taken from the experiment were divided into 84 runs, 67 runs taken with the beam on target and 17 runs for calibration and adjustment purposes. Since the fusion-evaporation reaction opens several reaction channels, a separation of the data in the corresponding channels is necessary. This process starts from the selection of the neutrons and the charged particles *(protons, alphas)* measured by NEDA + Neutron Wall and Diamant respectively. Then the data obtained are merged with the ones obtained from AGATA after imposing a time alignment between the detectors of the setup for coincidence measurements of the evaporated particles from the compound nucleus with the gamma-rays.

NEDA + Neutron Wall was used in the experiment as a neutron tagging instrument. For the discrimination of the neutrons from the gamma-rays which reach the crystals

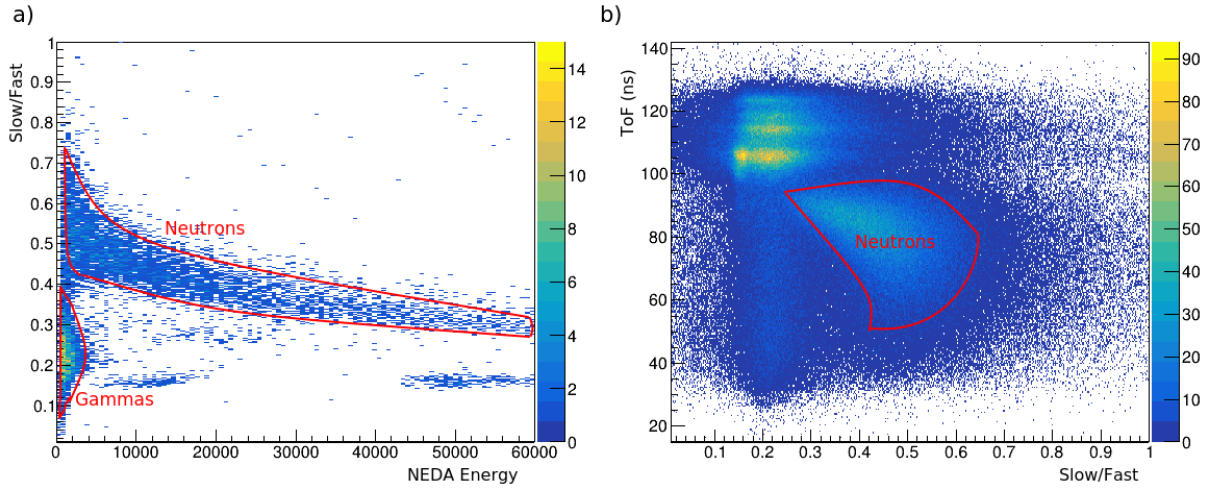

Figure 3.1: Neutron and gamma-ray discrimination

of the detector, algorithms based on the ratio of the integral of the fast and the slow component are used. The time of flight (ToF) of gamma-ray photons and the neutrons are different and this information can be used to distinguish them from each other. Two dimensional histograms as the ones shown in Figure 3.1 can be build after combining together these discrimination methods. These histograms allow one to properly set the particle gate for the neutron selection.

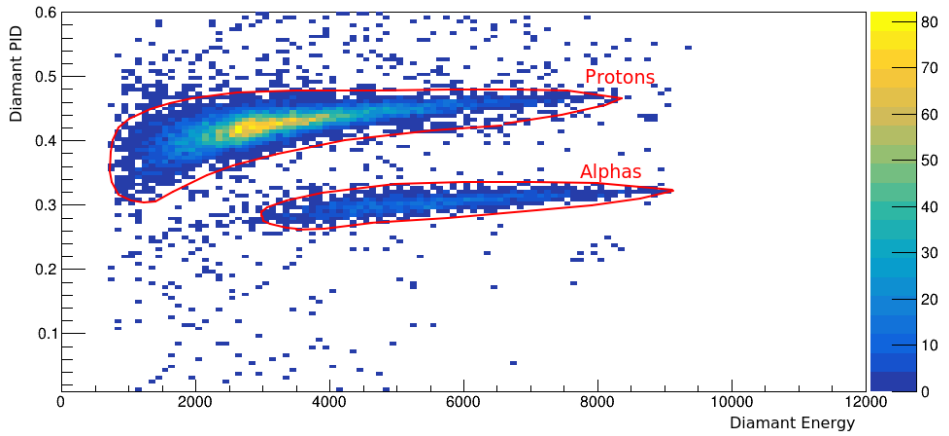

Figure 3.2: Protons and alpha particle discrimination

In this work Diamant was used as a tagging instrument for the protons and the alpha particles. In order to distinguish these two particles from each other for a proper selection of the channels, algorithms based on the ratio of the integrals of the fast and the slow component generated from the signal were used obtaining a "Diamant PID" variable. The two dimensional histogram in the Figure 3.2 was build by comparing the Diamant PID

variable with the energy measured. The two different regions corresponding to the alpha particles and the protons are marked in the figure. This helps on properly setting the gates for the selection of these particles.

All the events which pass through these selection processes are merged with the data recorded from AGATA. A time alignment is necessary to be set between the detectors on the merging process otherwise the events will be out of the coincidence window causing data loss. The time alignment between the detectors of the setup in the coincidence window is shown in the Figure 3.3.

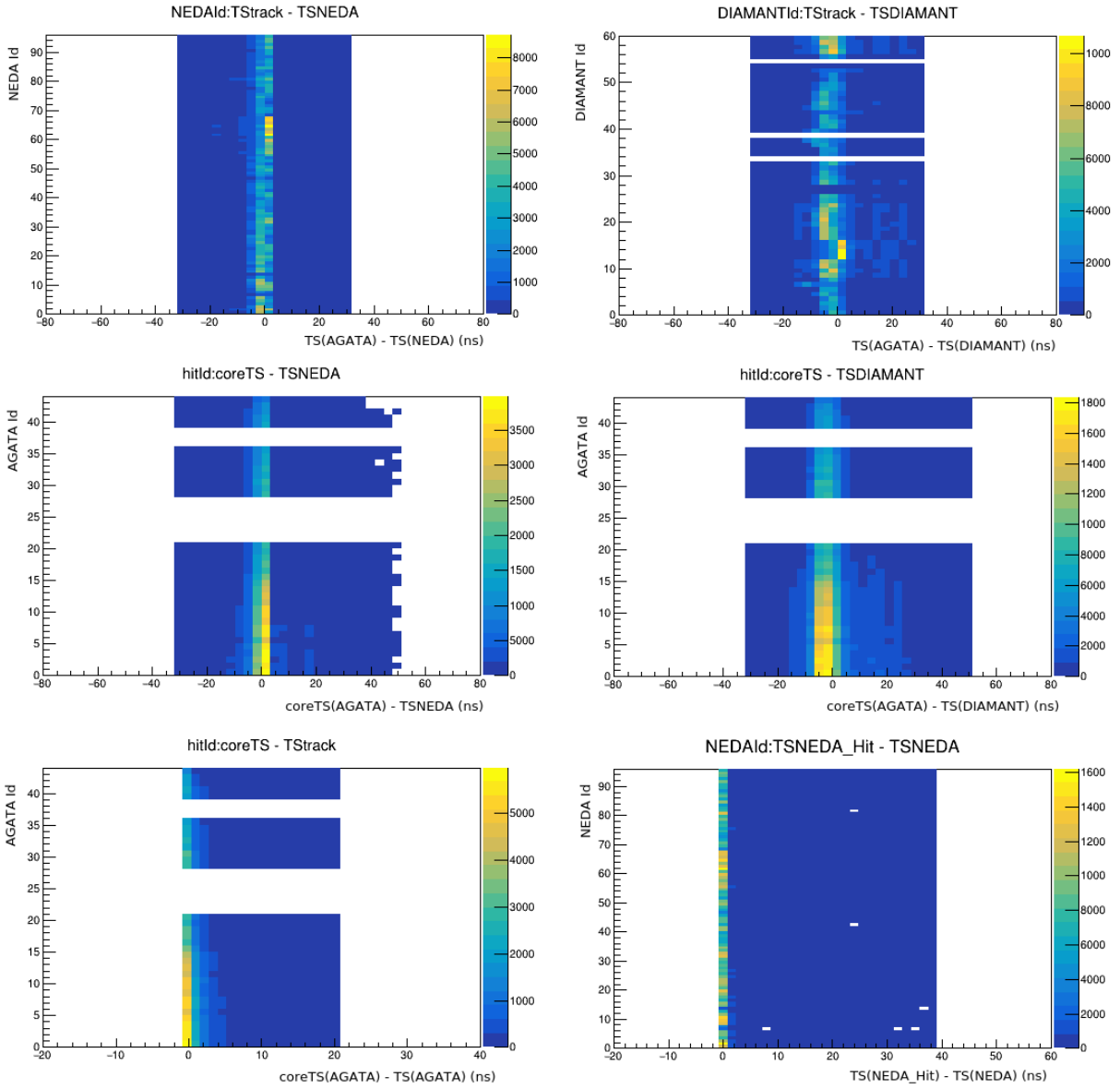

Figure 3.3: Time alignment in the coincidence window

After merging the data of NEDA, Diamant and AGATA the gamma-gamma matrices

for the corresponding channels are obtained. The Figure 3.4 shows the $\gamma - \gamma$ matrices of ^{46}Ti and ^{50}Cr.

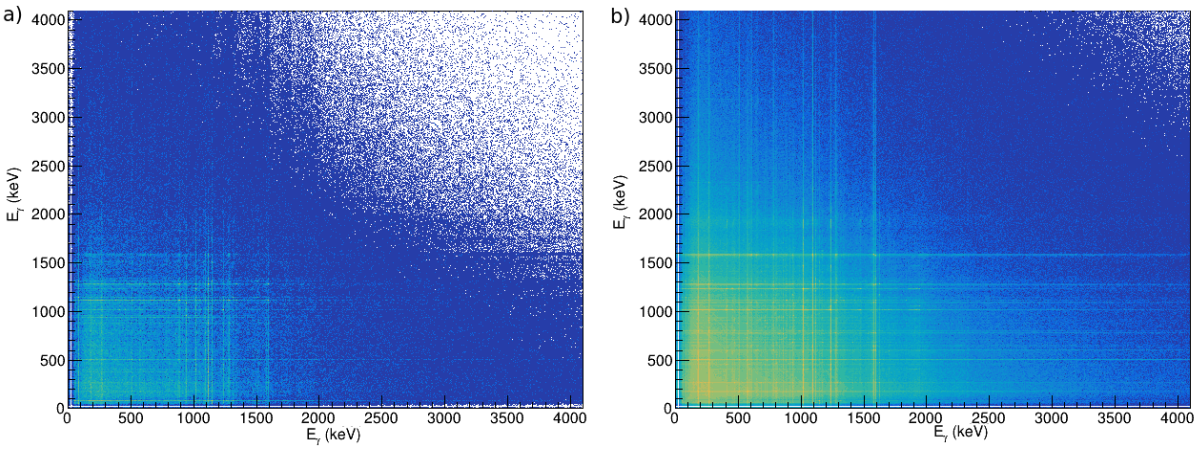

Figure 3.4: Gamma-gamma matrix of a) ^{46}Ti and b) ^{50}Cr obtained from the data reduction process

3.2 Efficiency of AGATA

There are several functions that can describe the efficiency of germanium detectors but none of them describe the efficiency of the segmented one. For AGATA the relative efficiency is more convenient to be used. The tracked and the untracked relative efficiency curves obtained by using standard calibration sources are represented in the Figure 3.5. The knowledge on the efficiency of AGATA is essential for the lifetime measurements.

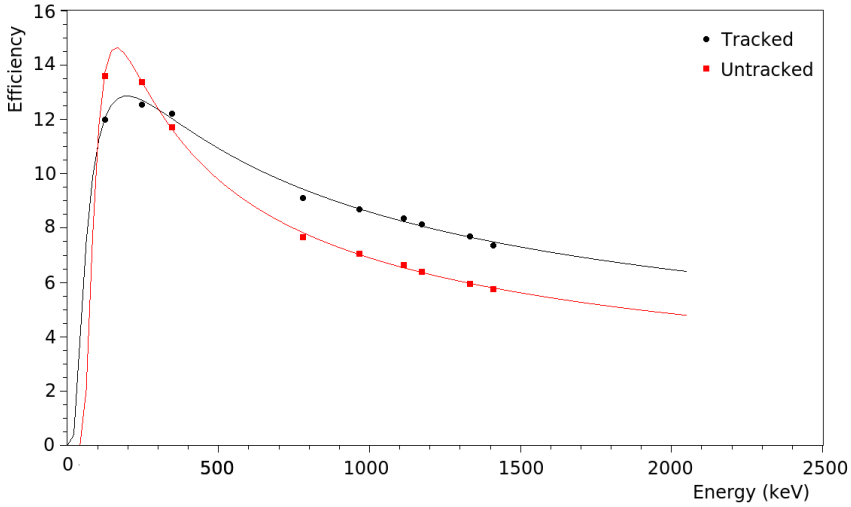

Figure 3.5: The tracked and untracked relative efficiency curves of AGATA

3.3 Particle efficiency estimation

For cross checking the merging process of the data, one can obtain the efficiencies of the detectors of the setup from the merged data. If the results obtained are comparable with the expected efficiencies then the merging process was performed properly.

During the experiment one of the runs was taken without putting any restrictions on the particle gates at trigger level. The data from this run together with the ones obtained by putting restrictions in one neutron, one proton and one alpha particle can be used for the efficiency estimation of the detectors, Neda and Diamant. The procedure for the efficiency estimation works as follow: The transition corresponding to a given channel is identified in both the gamma-ray spectra of the unrestricted run and the particle restricted one and the efficiency for particle tagging is estimated by the ratio of the area under the same peak.

$$E_f = \frac{A_1}{A_2} \tag{3.1}$$

where A_1 is the area of the peak in the particle restricted gamma-ray spectrum and A_2 is the area of the peak in the unrestricted spectrum.

The uncertainty of the efficiency is calculated from the formula below:

$$u(Ef) = Ef \cdot \sqrt{\left(\frac{u(A_1)}{A_1}\right)^2 + \left(\frac{u(A_2)}{A_2}\right)^2} \tag{3.2}$$

For the efficiency estimation of Diamant for one proton, in both the unrestricted and in the 1 proton restricted gamma spectrum, one "1p" channel has to be selected. ^{47}V is one of the strongest channels in the reaction and is a "1p1a" channel, which satisfies the condition mentioned above. To obtain the gamma ray spectrum of this channel it is possible to gate in both $\gamma - \gamma$ matrices in the 1149 keV peak ($11/2^+ \rightarrow 7/2^-$), which is the strongest transition of this nucleus. After gating on this peak, one can see in the projected spectra the gamma-rays measured in coincidence with it. One of the characteristic gamma-rays is the one in 1320 keV ($15/2^+ \rightarrow 1/2^-$), the area of which can be used for the efficiency estimation as mentioned above. The efficiency obtained for

the detection of one proton was calculated 38(2) % which is in good agreement with the efficiency we expect from the detection at one proton. In the Figure 3.6 the 1p restricted gamma ray spectrum is shown.

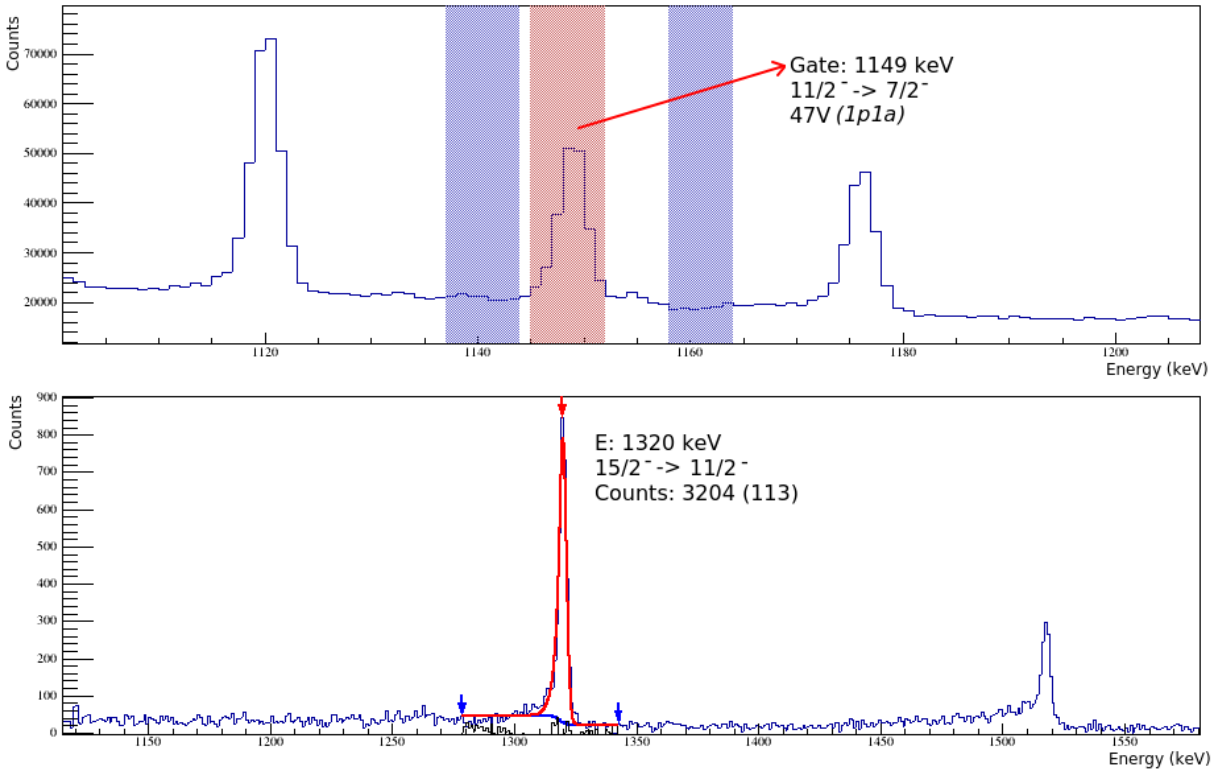

Figure 3.6: The 1 proton restricted spectrum gated in in 1149 keV ($11/2^- \rightarrow 7/2^-$) (^{47}V).

The same procedure was followed also for the efficiency estimation on the case of 1 neutron and 1 alpha particle. More details for the channels selected for the efficiency estimation in each particular case, the gates and the peaks chosen are given in the **Appendix A**.

The results obtained for the detection efficiency at 1 proton, 1 neutron and 1 alpha particle are shown below in the Table 3.1:

Table 3.1: Efficiency of detecting 1 neutron, 1 proton and 1 alpha particle

	Efficiency (%)
1 neutron	26(1)
1 proton	38(2)
1 alpha	26(1)

3.4 Data leakage estimation

Since in some cases the particle identification is ambiguous, it is possible that the data corresponding to a given channel are recorded to another one. For example, if the compound nucleus created from the reaction evaporates two protons and one alpha particle *(2p1a - ^{46}Ti channel)*, it is possible that the alpha particle is misidentified as a proton and so the gamma rays measured in coincidence are recorded in another channel, in this case a 3p channel which corresponds to ^{49}V nucleus.

The leakage of the data from one channel to another is estimated by the ratio between the area of a particular peak on the gamma-ray spectrum obtained from the unrestricted data with the area of the same peak on the restricted spectrum in a proton, neutron or at least one alpha. An effective leakage value is estimated in these calculations using the total statistics obtained with the regular trigger conditions.

For the leakage of the data in a "1n" channel, in the 1 neutron restricted gamma-gamma matrix a non-neutron related channel has to be selected. The strongest "non-neutron" channel is the one corresponding to ^{46}Ti (2p1a). Both the restricted and non-restricted $\gamma - \gamma$ matrices have been gated in the peak in 889 keV, the strongest transition of ^{46}Ti (2p1a), and then in the projected spectrum the area of the 1174 keV peak was used for the estimation of the leakage in the 1 neutron channel.

The same procedure was followed also for the leakage estimation in 1 alpha. More details for this particular case are given in **Appendix B**. The leakage of the data in a 1 proton channel could not be estimated since it was impossible to identify in the restricted 1p spectrum any "non-proton" channel.

The results obtained for the data leakage in the 1 neutron channel and 1 alpha channel are shown in the Table 3.2.

Table 3.2: Data leakage estimation in 1 neutron, 1 proton and 1 alpha channel

	Leaking estimation (%)
1 neutron	$(2.01 \pm 0.03)\%$
1 proton	-
1 alpha	$(0.61 \pm 0.01)\%$

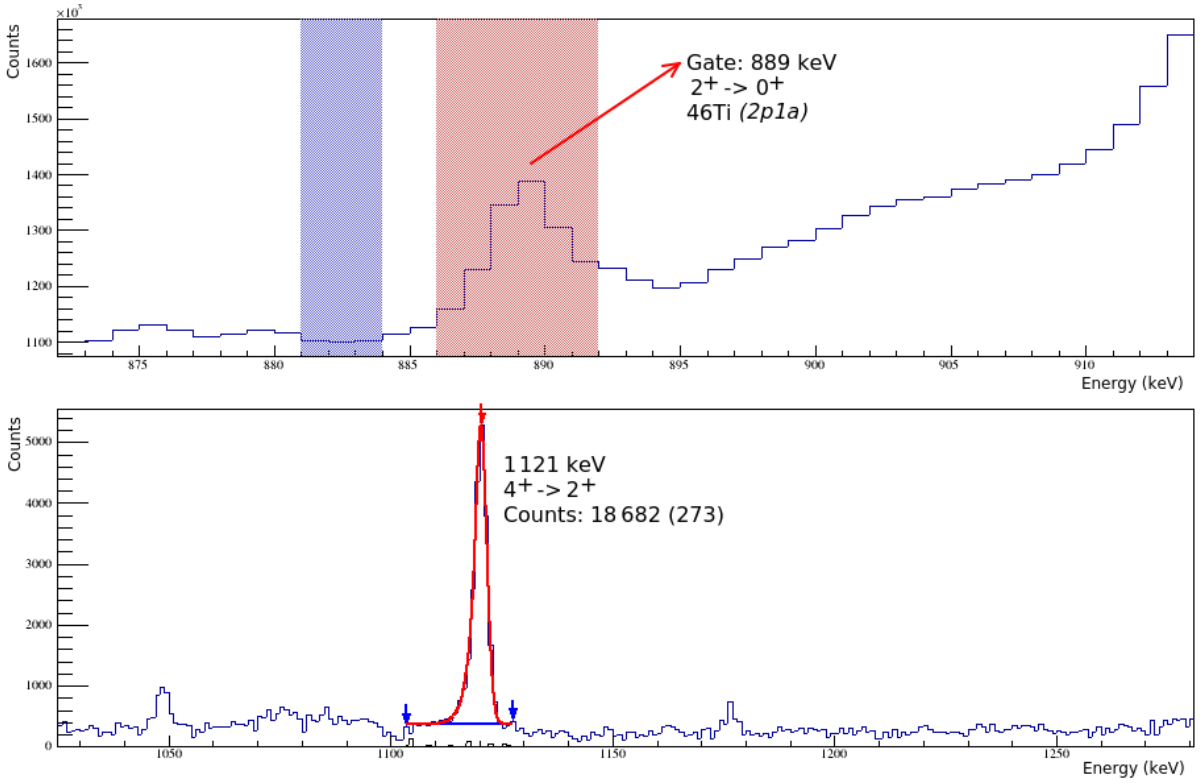

Figure 3.7: The 1 neutron restricted spectrum gated in 889 keV ($2^+ \rightarrow 0+$) (^{46}Ti)

3.5 Coincidence measurements in ^{46}Ti

^{46}Ti is produced following 2 protons and 1 alpha particle evaporation. All the gamma-rays measured in coincidence with two protons and one alpha particle have been recorded and the spectrum obtained is shown in the Figure 3.8.a. Due to the leakage of data from one channel to another this spectrum contains transitions which doesn't belong to ^{46}Ti. To obtain the gamma-ray spectrum of it one can gate in a transition of ^{46}Ti. The gated spectrum contains the gamma-rays measured in coincidence by the germanium crystals of AGATA with this transition. After identifying the peaks which correspond to ^{46}Ti by analysing the gamma-ray spectrum in Figure 3.8.a, a gate has been placed in the 889 keV peak, which is a ($2^+ \rightarrow 0^+$) transition of ^{46}Ti. The gated spectrum obtained from the gammas measured in coincidence with the 889 keV gamma photon is shown in Figure 3.8.b. Comparing the two spectra one can observe how much selective is this method and how much the background is reduced.

The intensities of each peak have been extracted from the experimental data and are represented in the Table 3.3. This information is very useful for understanding the

population of the excited states of ^{46}Ti from the reaction. The 511 keV peak originates the β decay of some of the products of the reaction and it is randomly recorded in coincidence with other gamma-rays. Peaks corresponding to ^{50}Cr with a very low intensity have been identified and are understood as being due to random coincidence.

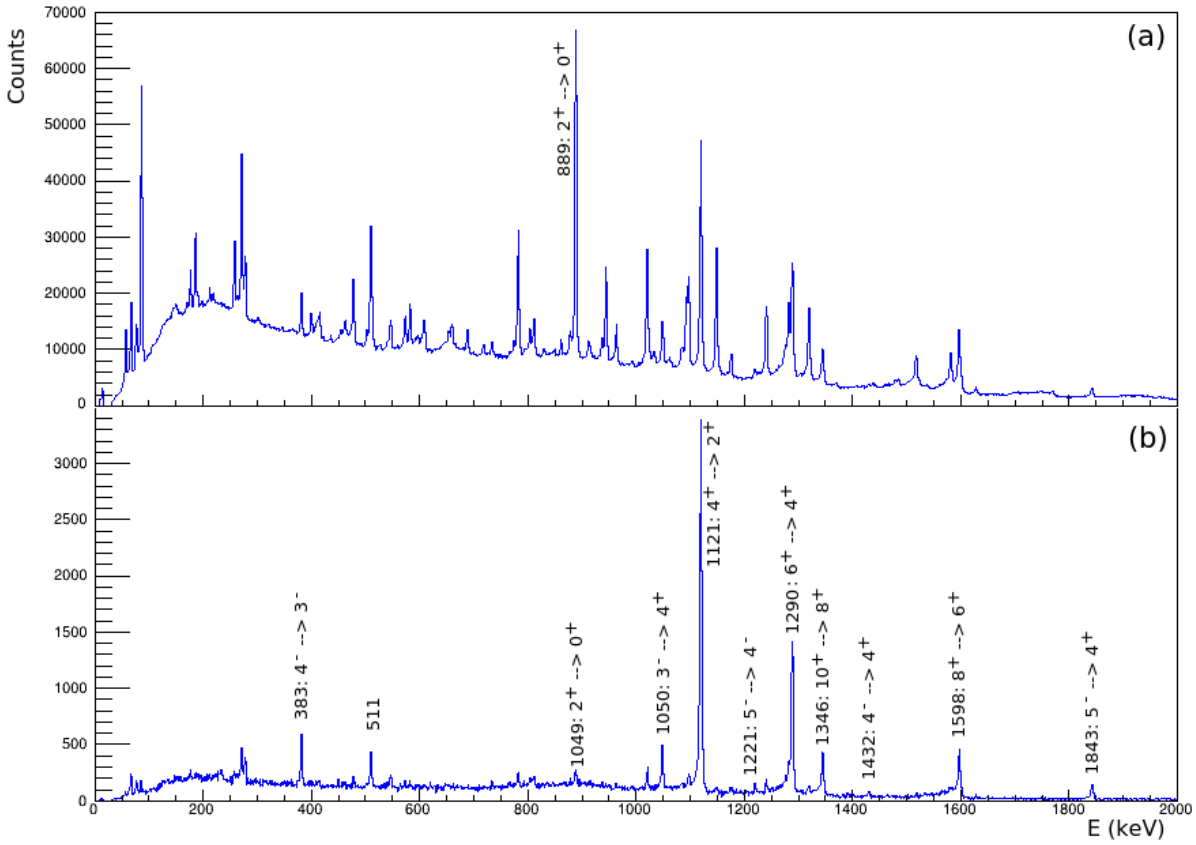

Figure 3.8: a) The ungated spectrum of 2p1a channel, b) the gated spectrum in 889 keV peak a ($2^+ \rightarrow 0^+$) transition of ^{46}Ti

In order to obtain the level scheme of ^{46}Ti it is important to measure in coincidence with other transitions. Some of the coincidence measurements performed are shown in the Figure 3.9. Measuring in higher transitions may allow the identification of other gamma peaks which were not observed on the gated spectrum in 889 keV. This will allow to build the level scheme of ^{46}Ti, a very important step for the proper population of the excited energy levels in the Monte Carlo simulations.

The measurements in coincidence with the 1346 keV shows peaks with energy 1598 keV, 1290 keV, 1121 keV and 889 keV. All these gamma-rays correspond to the same gamma cascade and all of them are E2 transitions. Gating in 1843 keV peak shows two

Table 3.3: The energy levels of ^{46}Ti, the gamma-rays and their intensities

E_{level} (keV)	J_i^π	J_f^π	E_γ (keV)	M	Intensity
2010	4+	2+	1121	E2	100
3030	3-	4+	1049	-	9
3298	6+	4+	1290	E2	50
3441	4-	3-	383	-	7
3852	5-	4+	1843	-	6
4662	6-	4-	1221	-	2
4898	8+	6+	1598	E2	22
6244	10+	8+	1346	E2	13

gammas in 1121 keV and 889 keV. Since the 1843 keV gamma doesn't correspond to the same cascade as the one mentioned above, the peak we see in 1346 keV may be coming from another energy level which decays also by emitting the same gamma-ray. This means that two energy levels are feeding the gamma peak observed in the spectrum in 1346 keV. The coincidence measurement in 1049 keV and 383 keV shows the same gamma-ray peaks which means they correspond to the same cascade.

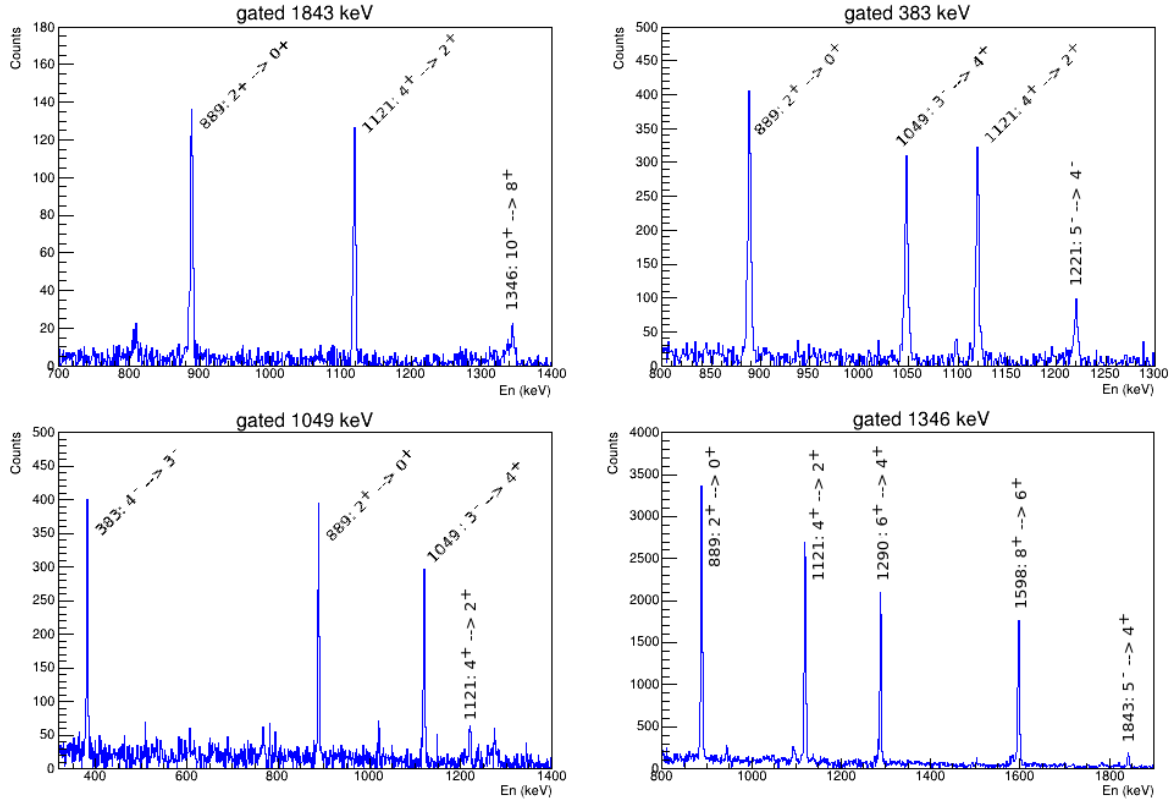

Figure 3.9: Coincidence spectra in different transitions of ^{46}Ti

3.6 Level scheme of ^{46}Ti

By analysing the gamma-ray spectrum and the coincidence measurements it was possible to construct the level scheme of ^{46}Ti which is shown in the Figure 3.10. In red color are represented the energy levels for which our lifetime measurement method is sensitive.

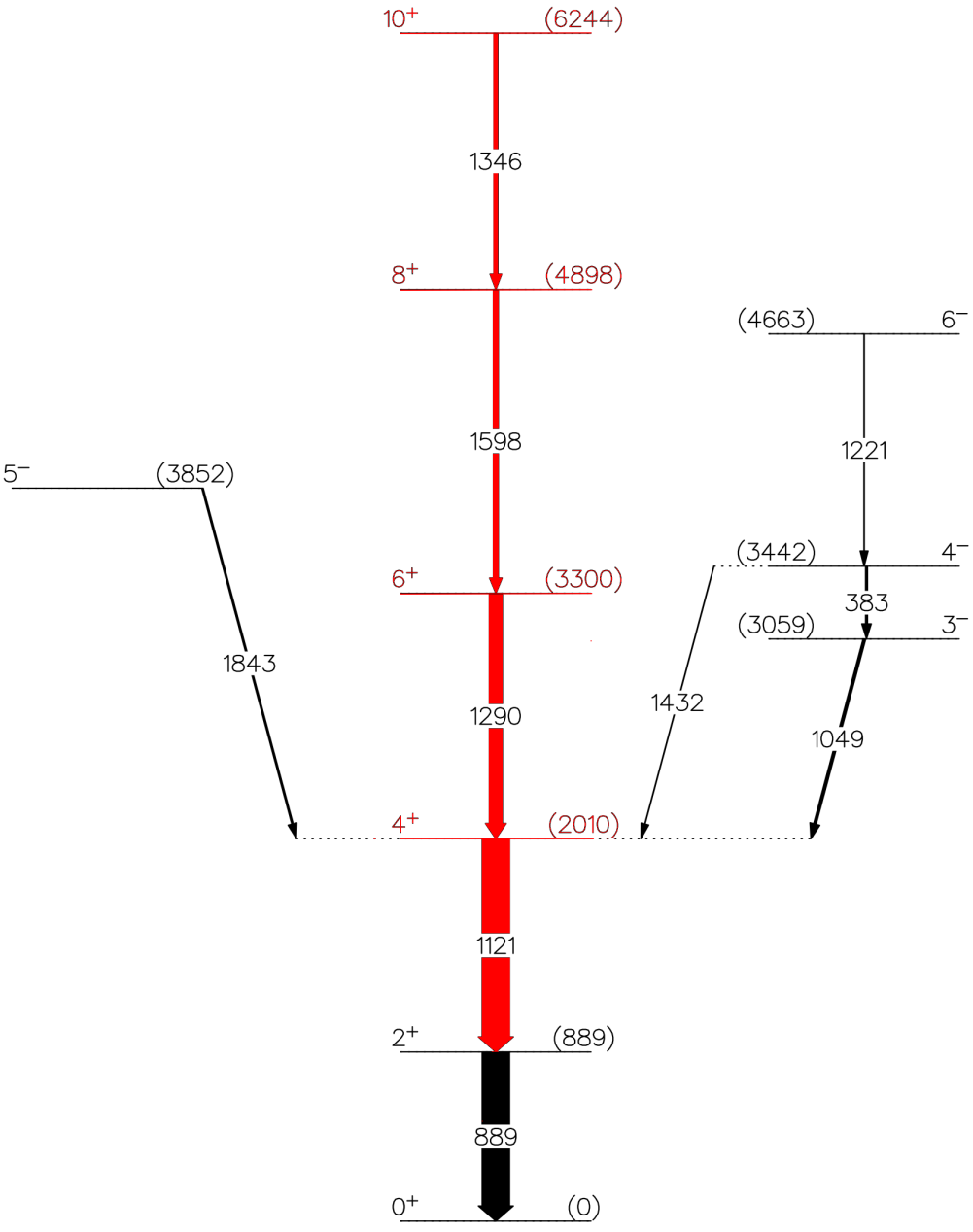

Figure 3.10: The level scheme of ^{46}Ti constructed from experimental data

3.7 Coincidence measurements in ^{50}Cr

^{50}Cr is produced following 2 protons evaporation. The spectrum obtained from the coincidence measurements of the gamma-rays with the two protons is shown in the Figure 3.11.a. The same procedure has been followed as we described in the case of ^{46}Ti. After identifying the peaks corresponding to ^{50}Cr a gamma coincidence measurement has been performed by gating on the 783 keV a $(2^+ \rightarrow 0^+)$ transition and the strongest one of ^{50}Cr. The gated spectrum which now shows the gamma-rays measured in coincidence with the 783 keV gamma-ray photon is shown in the Figure 3.11.b.

The peaks which correspond to ^{50}Cr have been identified and their intensities are given in the Table 3.4. The 511 keV peak which appears in the spectrum is coming from the β decay of some of the products of the reaction.

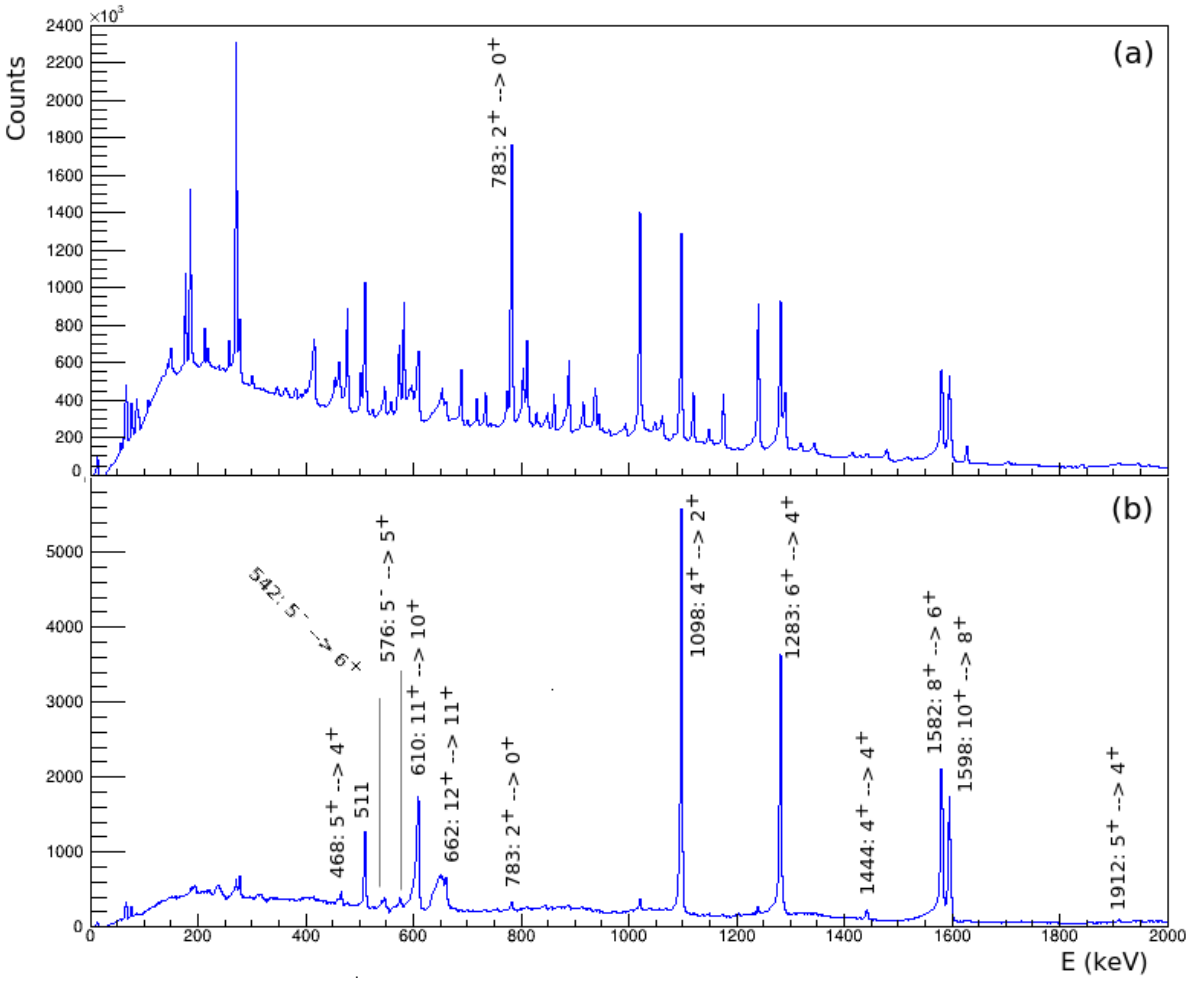

Figure 3.11: a) The ungated spectrum of 2p channel, b) the gated spectrum in 783 keV peak a $(2^+ \rightarrow 0^+)$ transition of ^{50}Cr

To reconstruct the level scheme of ^{50}Cr, gating in the strongest transition (889 keV peak) is not sufficient. Measuring in coincidence with other transitions may help on identifying other gamma peaks with a small intensity corresponding to other cascades. In the Figure 3.12 the energy spectra obtained from coincidence measurements in different transitions of ^{50}Cr are shown.

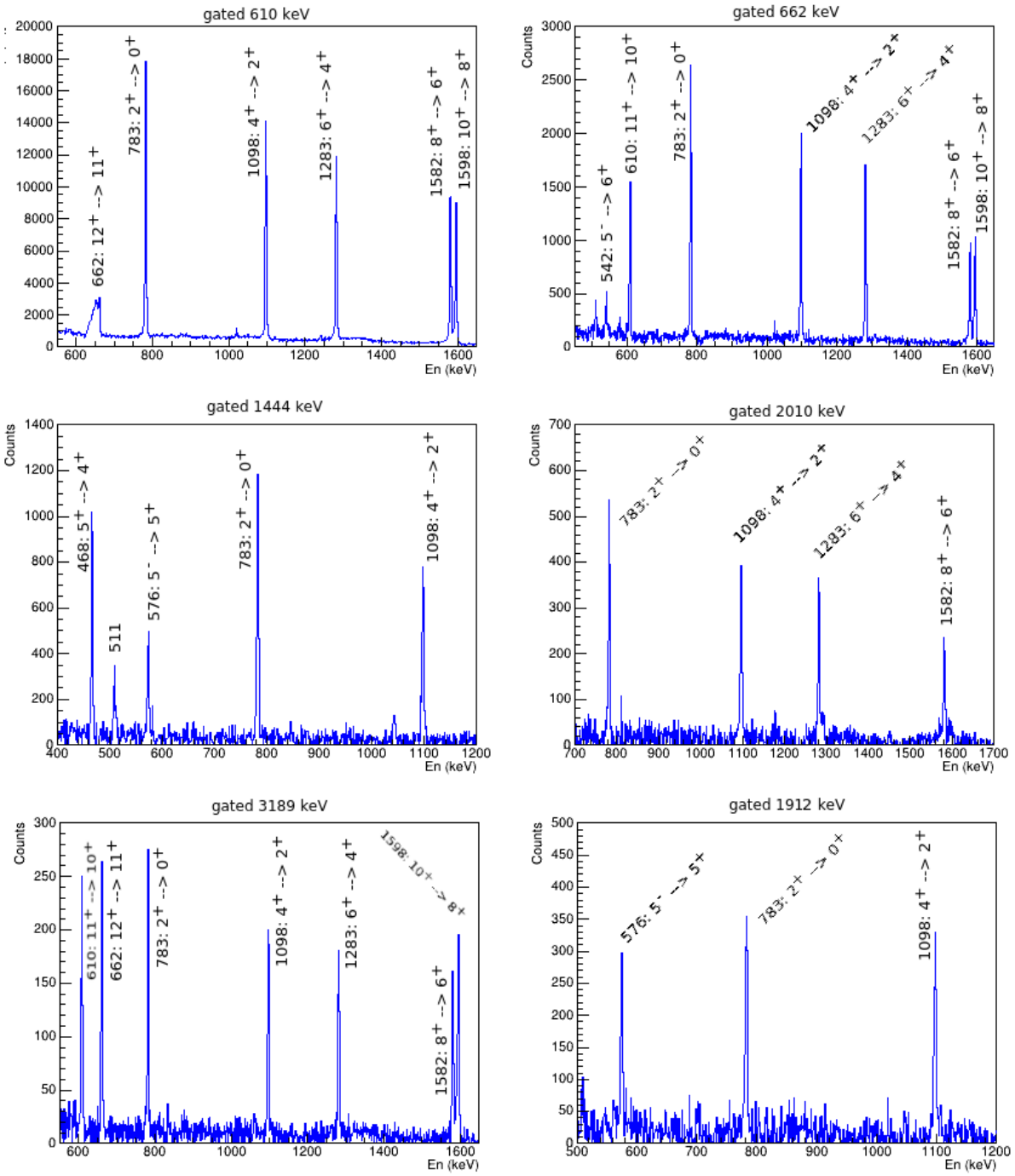

Figure 3.12: Coincidence spectra in different transitions of ^{50}Cr

The coincidence measurement with the 662 keV shows an interesting spectrum where

Table 3.4: The energy levels of ^{50}Cr, the gamma rays and their intensities

E_{level} (keV)	J_i^π	J_f^π	E_γ (keV)	M	Intensity
1881	4+	2+	1098	E2	100
3164	6+	4+	1283	E2	79
3324	4+	4+	1444	-	3
3793	5+	4+	468	-	3
		4+	1912	-	1
4746	8+	6+	1582	E2	55
6343	10+	8+	1598	E2	38
6953	11+	10+	610	M1	36
7615	12+	11+	662	M1	49

one can identify the peaks coming not only from the cascade where this gamma-ray belong but also the presence of the 575 keV peak in the spectrum it shows that this peak is being fed by two energy levels of ^{50}Cr which both decay by emitting gamma-rays with 662 keV energy. This is important to be implemented also in the simulations for the lifetime measurements. It can be seen that the 662 keV peak in the spectrum is a bump followed by a small sharp peak. The 7615 keV energy level has a short lifetime compared with the 3825 keV energy level. This means that the former one is contributing in the bump and the other one in the sharp peak next to it.

The coincidence measurement in the 3189 keV peak shows the gamma-rays as represented in Figure 3.12. This gamma is coming from the decay of the 10804 keV energy level, a 13^+ state. This peak in the 889 keV gated spectrum is hidden by the background.

The coincidence measurement with the 2010 keV peak, which it was present also in the gated spectrum in the 889 keV peak showed that this peak is coming from the same cascade as the E2 transitions shown in the level scheme and correspond to the decay of the second 10^+ level. The 6756 keV energy level decays by emitting this gamma-ray.

The gated spectrum in 1444 keV and in the 1912 keV peak shows transitions corresponding to another cascade. Both of them have the 576 keV peak in common, which means that one of the energy levels, the 3793 keV energy level, is decaying by emitting two gamma rays.

3.8 Level scheme of ^{50}Cr

The level scheme of ^{50}Cr has been reconstructed by analysing the gamma-ray spectra obtained by coincidence measurements in different transitions and it is shown in the Figure 3.13. The red part of the level scheme represents the energy levels for which our lifetime measurement method is sensitive.

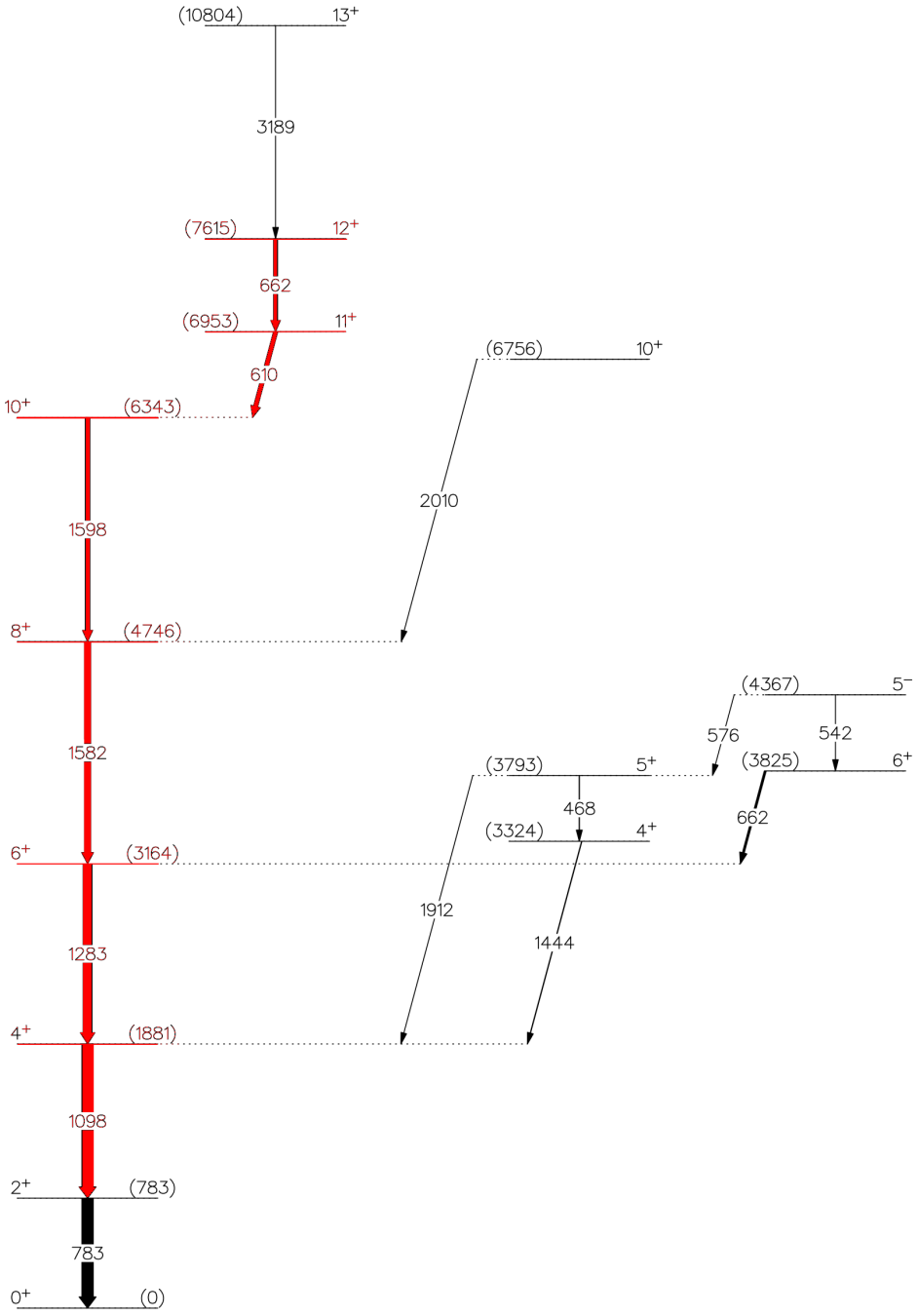

Figure 3.13: The level scheme of ^{50}Cr constructed from experimental data

3.9 Lifetime measurements

The lifetimes are 'extracted' from the experimental data via a comparison of the gamma-ray spectrum with a model calculation. A Monte Carlo Simulation code based on GEANT4 has been use to produce the model spectrum for the comparison. There are several parameters that need to be set properly in the code in order to be able to reproduce as good as possible the experimental spectrum:

- The population of the energy levels excited in the reaction
- The lifetimes of the energy levels
- The background parameters

The exact population of the energy levels in the reaction it can be determined with limited precision and this leads to uncertainties in our simulated spectrum affecting the lifetime determination. In order to properly set the population of the energy levels in the simulations it is necessary to reconstruct the level scheme of the nucleus of interest and extract the experimental intensities for each of the gamma peaks identified in the corresponding spectrum. The population for the energy levels of ^{46}Ti and ^{50}Cr which were used in the simulations are given in the Table 3.5.

Table 3.5: The population of the energy levels in the Monte Carlo code

^{46}Ti		^{50}Cr	
E_{level} (keV)	Population	E_{level} (keV)	Population
2010	14.71	1881	4.36
3059	1.84	3164	2.86
3299	13.25	3792	0.75
3441	2.67	3825	1.94
3852	2.67	4745	4.16
4662	0.77	6341	4.46
4897	3.87	6951	0.3
6242	7.9	7613	7.79

The background parameters can be changed by the user until a good agreement between the background level of the simulated spectrum and the experimental one is

achieved. The most important feature of this Monte Carlo code is that the excited nucleus decays by following complicated gamma level schemes taking into consideration also the lifetimes of the energy levels. The user can change these ones until the lineshapes are properly reproduced. This is how then one conclude about the lifetimes of the energy levels.

3.9.1 Lifetime measurements in ^{46}Ti

A comparison of the experimental gamma-ray spectrum of ^{46}Ti and the simulated one both gated in 889 keV peak it is shown in the Figure 3.14. Five million events were simulated to achieve a good statistics on the simulated data. The normalization coefficient was obtained by the ratio of the area under the peak in 1121 keV in both the gated spectra.

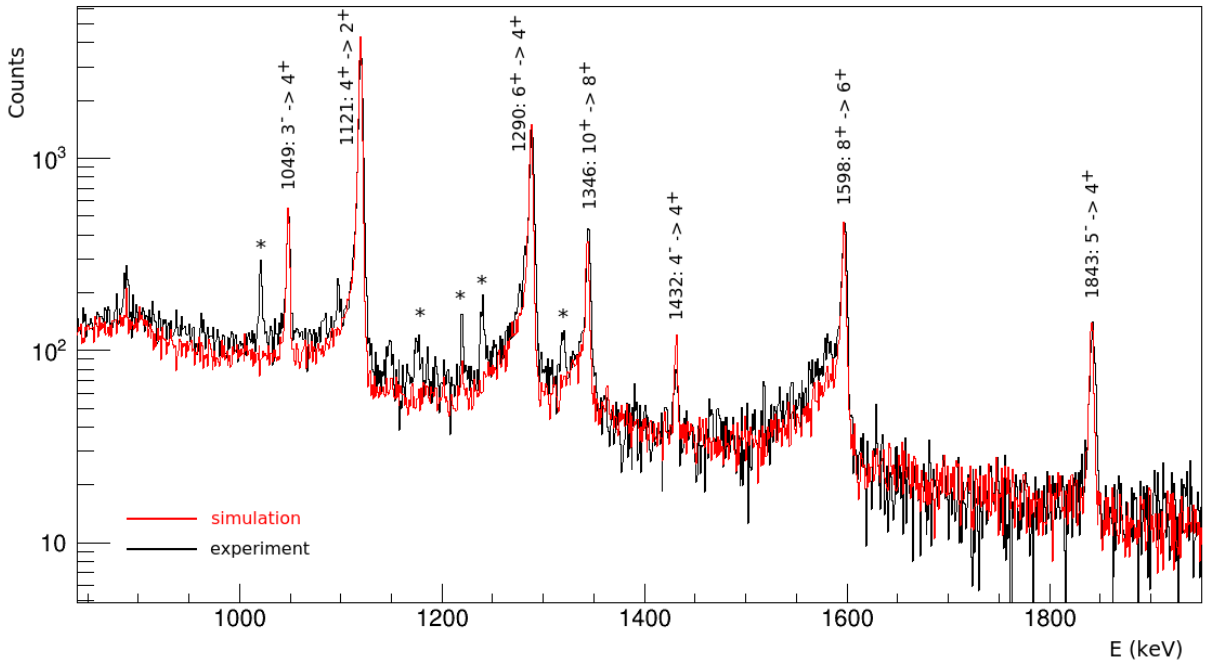

Figure 3.14: A comparison of the simulated spectrum of ^{46}Ti with the experimental one. Peaks coming from the background are marked with (*).

The 10^+ state with energy 6244 keV is the highest energy level in the case of the ^{46}Ti nucleus and sensitive to the lifetime measurement. This level decays in the 8^+ state by a pure E2 transition emitting a gamma-ray with energy 1346 keV. The 1346 keV peak can be seen in the spectrum with a tail in the left side which is well reproduced from the simulation. The lifetime measured from the experiment is $\tau = 1.21(7)$ ps. This value is

Table 3.6: The measured lifetimes of the energy levels of ^{46}Ti *(preliminary results)* compared with the results from literature

E_{level} (keV)	J^{π}	τ exp (ps)	τ lit. (ps)	E_{γ} (keV)
6244	10+	1.21(7)	2.5(6)[a]	1346
			1.68(15)[b]	
4898	8+	0.36(10)	1.33(33)[a]	1598
			0.51(5)[b]	
3300	6+	0.97(23)	1.34(13)[b]	1290
2010	4+	1.44(43)	2.01(23)[b]	1121
			2.00(15)[c]	

shorter than the ones reported in previous experiments [5] [8].

The 8^+ state with energy 4898 keV decays by a pure E2 transition emitting a gamma-ray with energy 1598 keV which is present in the spectrum. This lineshape is well reproduced from the simulation and the lifetime of this level was estimated to be $\tau = 0.36(10)$ ps. This value is close with the previous measurement as reported in [8] but is quite different from another measurement reported in [5].

Also in the spectrum there can be seen two other lineshapes located in the 1290 keV and 1121 keV, resulting from the decay of the 3300 keV and the 2010 keV energy levels respectively. The tails are well reproduced from the simulations in both cases. The estimated values for the lifetime are $\tau = 0.97(23)$ ps for the 6^+ state and $\tau = 1.44(43)$ ps for the 4^+ state. In both cases these lifetimes are shorter compared with ones reported in [8] or [27].

In the Figure 3.14 one can notice small peaks which appear in the experimental spectrum but not in the simulated one. These peaks have been identified as corresponding to ^{50}Cr. As we have discussed earlier in this chapter, the leakage of the data from one channel to another is possible because of the efficiency of the ancillary detectors (NEDA, Diamant). The intensity of these peaks is small and it doesn't influence the lineshapes of ^{46}Ti.

[a] Reference [5]
[b] Reference [8]
[c] Reference [27]

The 2^+ and others states with negative parities could not be measured by our method because of the very low intensities or because of their lifetimes out of the range that can be measured by DSAM.

In the Table 3.6 the lifetimes of the energy levels of ^{46}Ti measured in this experiment are compared with previously reported values.

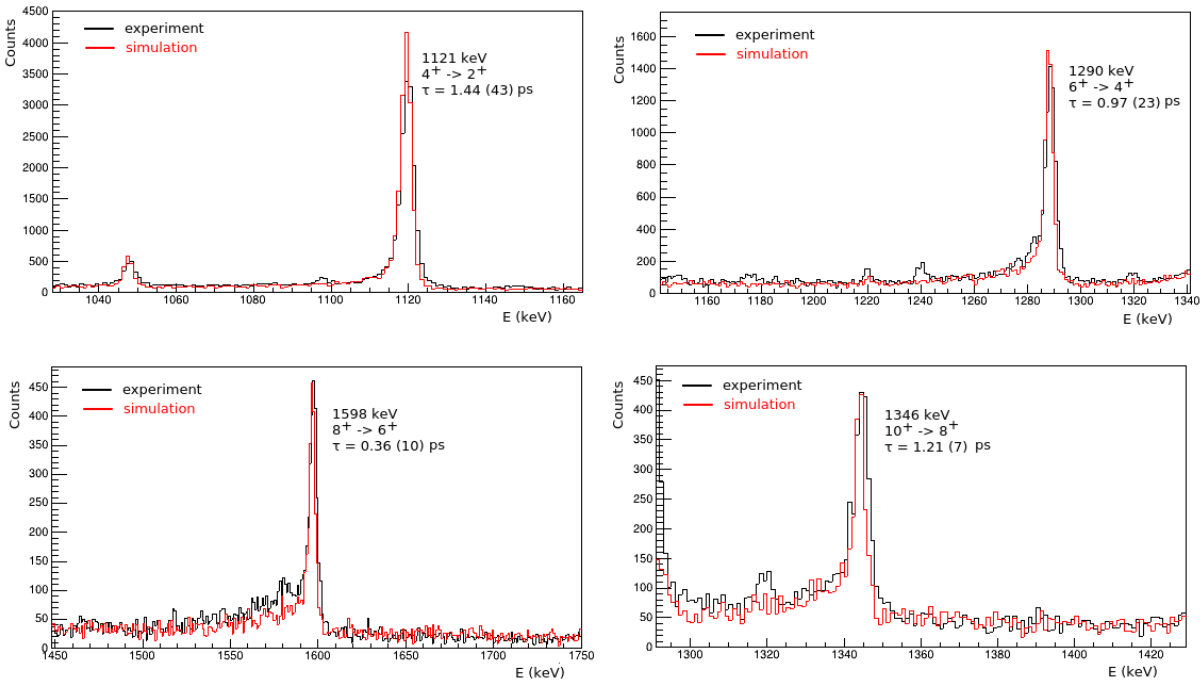

Figure 3.15: Comparison between the simulated and experimental data of ^{46}Ti

3.9.2 Lifetime measurements in ^{50}Cr

The same procedure as described in the case of ^{46}Ti has been followed also for the ^{50}Cr nucleus. After building the level scheme and getting the intensities of the identified peaks, each energy level was associated with the corresponding population numbers as shown in the Table 3.5. Simulations have been performed by changing the lifetimes of the energy levels until a good agreement between the simulated spectrum and the experimental one was obtained. In the Figure 3.16 a comparison of the two spectra is shown. Both of the spectra have been gated in the 783 keV peak. The normalization coefficient of the simulated spectrum was obtained from the ratio of the area under the 1098 keV peak of both spectra.

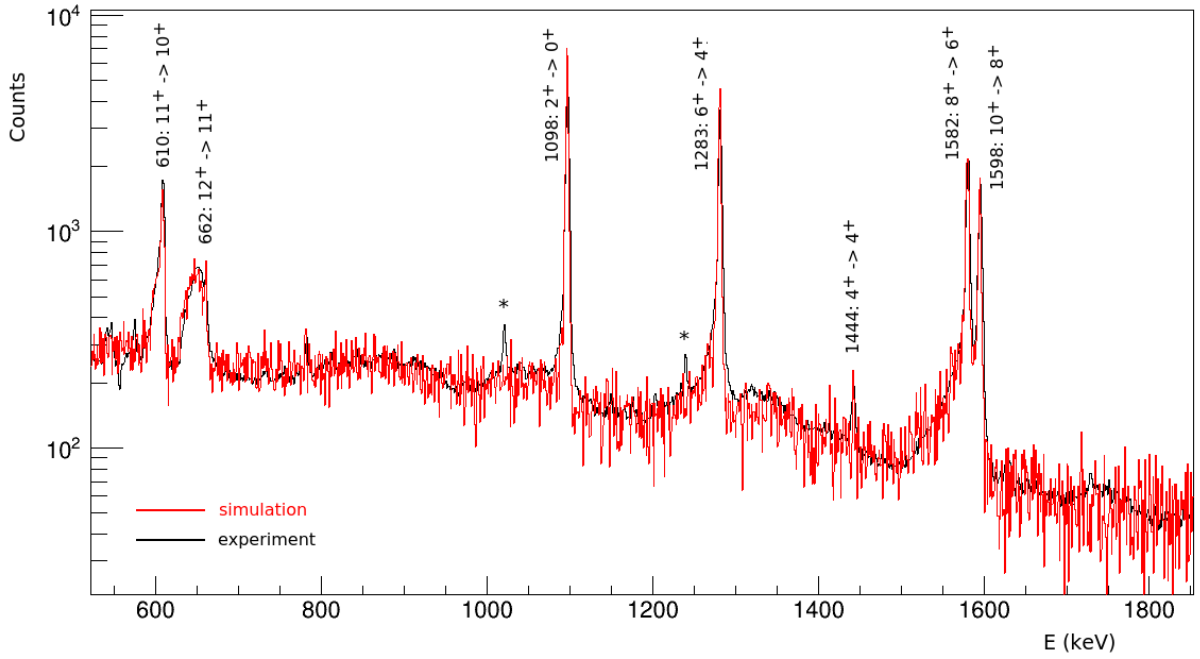

Figure 3.16: Comparison of the simulated spectrum of ^{50}Cr with the experimental one, both of them gated in the 783 keV peak. The peaks coming from the background are marked (*).

The 12^+ state with energy 7615 keV is the highest energy level of ^{50}Cr sensitive to the lifetime measurement. This state decays in the 11^+ level by emitting a gamma-ray with energy 662 keV. The $(12^+ \rightarrow 11^+)$ is a pure M1 transition. Since the lifetime of the 12^+ state is very short, due to the Doppler effect, these gamma-rays contribute in the spectrum on the bump shape located at around 600 keV which is well reproduced also from the simulation as it can be seen in the spectrum. In the right side of the bump is located a small sharp peak which actually is a contribution of another excited nuclear energy level with a longer lifetime, the 3825 keV level. The presence of this peak next to the bump was shown in the coincidence measurements early in this chapter. The estimated lifetime of the 12^+ energy level in our experiment is $\tau = 0.19(7)$ ps. This result is similar to the previously measured lifetimes reported in [5] [9].

The 11^+ state, which is fed mainly by the 12^+ state, decays by emitting a gamma with energy 610 keV, a pure M1 transition on the 10^+ state. This peak is present in the spectrum and because of the short lifetime has a tail in the left side. The lifetime measured from our experiment is $\tau = 0.56(10)$. This lifetime is shorter compared with ones reported from previous experiments [5] [9].

Table 3.7: The measured lifetimes of the energy levels of ^{50}Cr *(preliminary results)* and compared with the results from literature

E_{level} (keV)	J^{π}	τ exp (ps)	τ lit. (ps)	E_{γ} (keV)
7615	12+	0.19(7)	0.24(3)[a]	662
			0.160(15)[b]	
6953	11+	0.56(10)	0.83(14)[a]	610
			0.7(6)[b]	
6343	10+	1.05(17)	1.1(2)[b]	1598
4746	8+	0.4(1)	0.4(11)[b]	1582
3164	6+	1.00(25)	1.0(2)[b]	1283
1881	4+	2.4(3)	2.5(7)[b]	1098

The next two lineshapes very close to each other, the one in 1598 keV and 1582 keV are a result of the decay of the 10^+ and the 8^+ state respectively. It is important to note that it is difficult to discuss the lifetimes of this two energy levels since the lineshapes are very close and they may affect the tail of each other, making it complicated to extract the lifetimes of the corresponding energy levels. Different parameters combinations may lead to different lifetimes, so the result is not unique. Simulating with the lifetimes around the values which we got from previous measurements as a reference [9] seems to work very well and reproduce the lineshapes in a quite good agreement. For the 10^+ state a lifetime $\tau = 1.05(17)$ ps was measured and for the 8^+ state $\tau = 0.4(1)$ ps.

The two other peaks located in the 1098 keV and 1289 keV, resulting from pure E2 transitions ($4^+ \rightarrow 2^+$) and ($6^+ \rightarrow 4^+$) respectively, appear in the spectrum with a tail on the left side, an effect of their lifetime. The lifetime of the 6^+ state was found to be $\tau = 1.00(25)$ ps and the lifetime of the 4^+ state $\tau = 2.4(3)$ ps. Both the values are in a good agreement with the results obtained in[9].

The lifetimes obtained from the experimental measurement and their comparison with the previously reported results are shown in the Table 3.7. A comparison of the experimental data and the simulation for each of the lineshapes is given in Figure 3.17.

The peak located at 1022 keV which appears in the experimental spectrum but is not reproduced on the simulation is a sum peak of two 511 keV gammas which arrive in

[a] Comparison with [5]
[b] Comparison with [9]

the same time in the crystal of the detector.

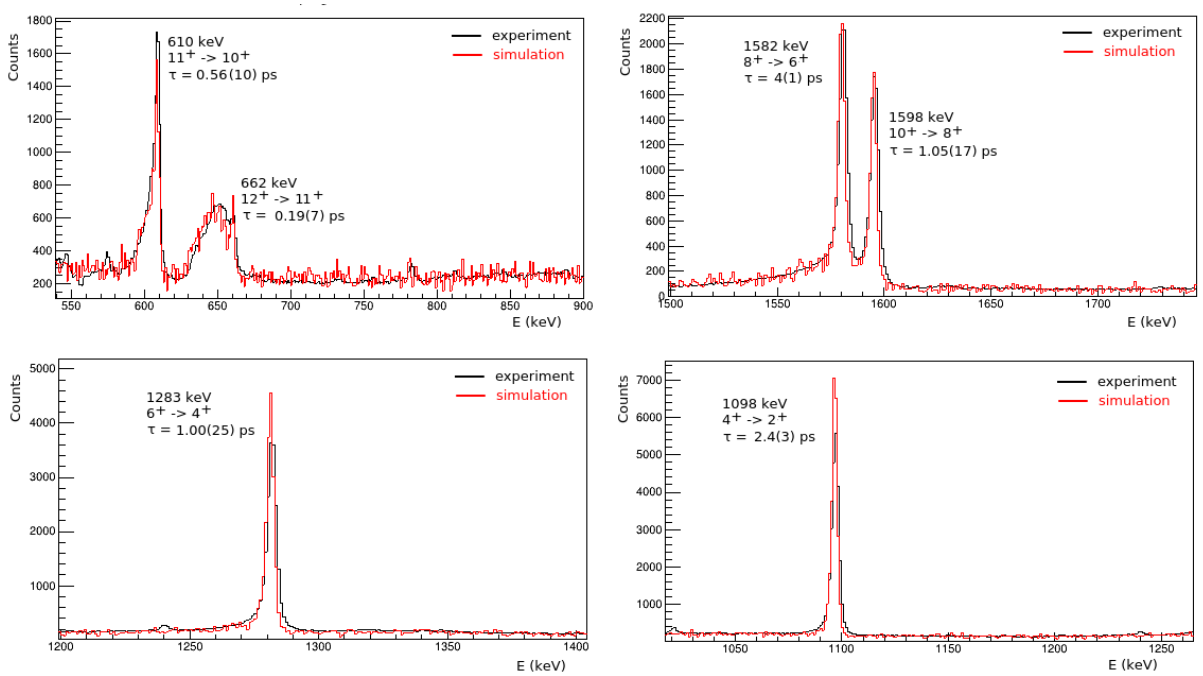

Figure 3.17: Comparison between the simulated and experimental data for ^{50}Cr

Chapter 4

Results and discussions

In this chapter the transition probabilities obtained from the lifetime measurements of the levels in ^{46}Ti and ^{50}Cr are discussed in comparison with the ones obtained from shell model calculations.

4.1 Transition probabilities in ^{46}Ti

As it was mentioned in the first chapter, the quality of the shell model calculations for the nuclei in the $1f_{7/2}$ shell has improved during the past decades due to the spectroscopic data available for the nuclei in this region. The experimental results obtained in this work illustrated in chapter 3 are going to be compared with the ones obtained from shell model calculations based on the KB3G [28] and GXPF1A [29] interactions. The model space comprises the full pf shell coupled to a ^{40}Ca core. For the calculations of transition probabilities effective charges $1.5e$ and $0.5e$ were used for the valence protons and neutrons respectively.

A comparison of the experimental excitation energies with the calculated values from the models for the first 2^+, 4^+, 6^+, 8^+ and 10^+ states is shown in the Figure 4.1.a. The energy of the low spin states is well reproduced, but both interactions underestimate the energy of the high spin states by few hundreds of keV. As it can be seen in the Figure 4.1.b even though the model doesn't calculate the same values for the energy of the gamma-rays, their behaviour with respect to the spin of the states is the same as the experimental

ones. The energy of the gamma-rays increase with the spin up to 8^+ state. In the 10^+ state there is a drop compared with the previous transitions. This drop of the energy of the gamma-rays originating from a high spin state is an indication of the changes in the nuclear structure.

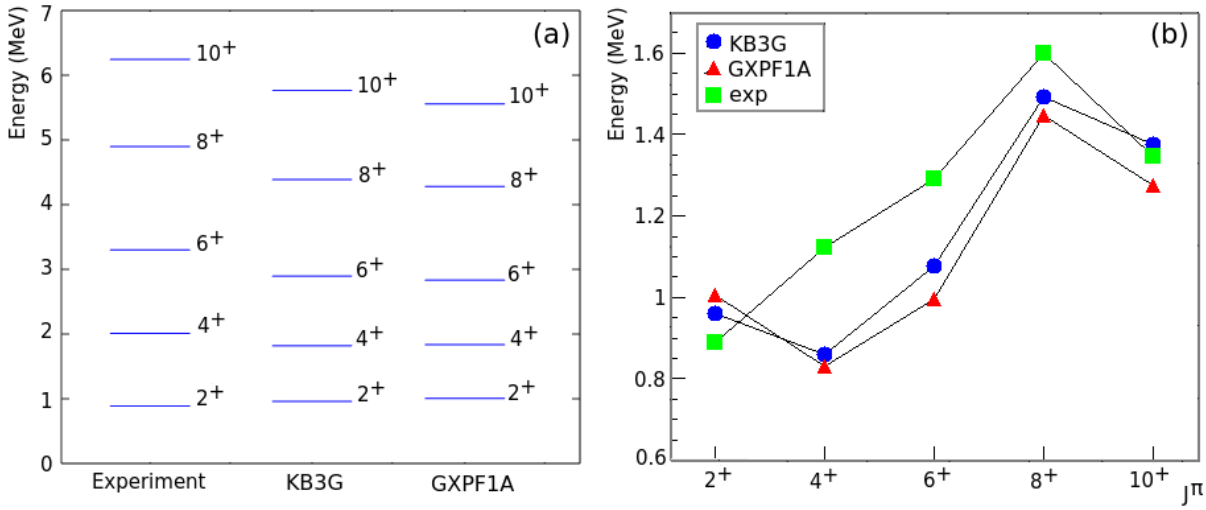

Figure 4.1: a) Comparison of the experimental excitation energies of ^{46}Ti with the calculated ones based on the KB3G and GXPF1A interactions b) Comparison of the energy of the depopulating transitions along the yrast states measured experimentally with the ones obtained from the calculations

From the lifetimes which were obtained experimentally it is possible to obtain the reduced transition probabilities by using the formula 4.1 represented below which correspond to the transition probabilities for E2 transitions. The first 2^+,4^+,6^+,8^+ and 10^+ states of ^{46}Ti all decay by pure E2 transitions.

$$B(E2) = \frac{1}{1.223 \cdot 10^9 \cdot E_\gamma^5 \cdot \tau} \tag{4.1}$$

The B(E2) is the reduced transition probability in e^2fm^4, E_γ is the energy of the gamma released in the corresponding transition in MeV and τ is the lifetime of the initial energy level in seconds.

The Table 4.1 shows the reduced transition probabilities obtained from the experimental lifetimes. A comparison of the experimental transition probabilities with the ones obtained from the calculations is represented in the Figure 4.2.

As it can be seen from the Figure 4.2 the transition probabilities obtained from

Table 4.1: The reduced transition probabilities B(E2) of ^{46}Ti

Transition	E_γ (keV)	τ (ps)	B(E2) (e^2fm^4)
$10^+ \rightarrow 8^+$	1346	1.21 (7)	153 (9)
$8^+ \rightarrow 6^+$	1598	0.35 (10)	218 (61)
$6^+ \rightarrow 4^+$	1290	0.97 (23)	237 (56)
$4^+ \rightarrow 2^+$	1121	1.44 (43)	320 (96)

the experimental lifetime estimation are quite different from the ones obtained from the calculations. The B(E2,J $\rightarrow$ J-2) of the 6^+, 8^+ and 10^+ have the same tendency as the ones from the shell model calculations, but the values of the 4^+ are quite different. We mentioned in the beginning of this section the fact that the calculations do not reproduce very well the energies of the gamma rays and also the energy of the levels. The transition probabilities have a strong dependence also in these quantities, that's why it is expected to have this difference between the values calculated theoretically with the ones obtained from the experiment.

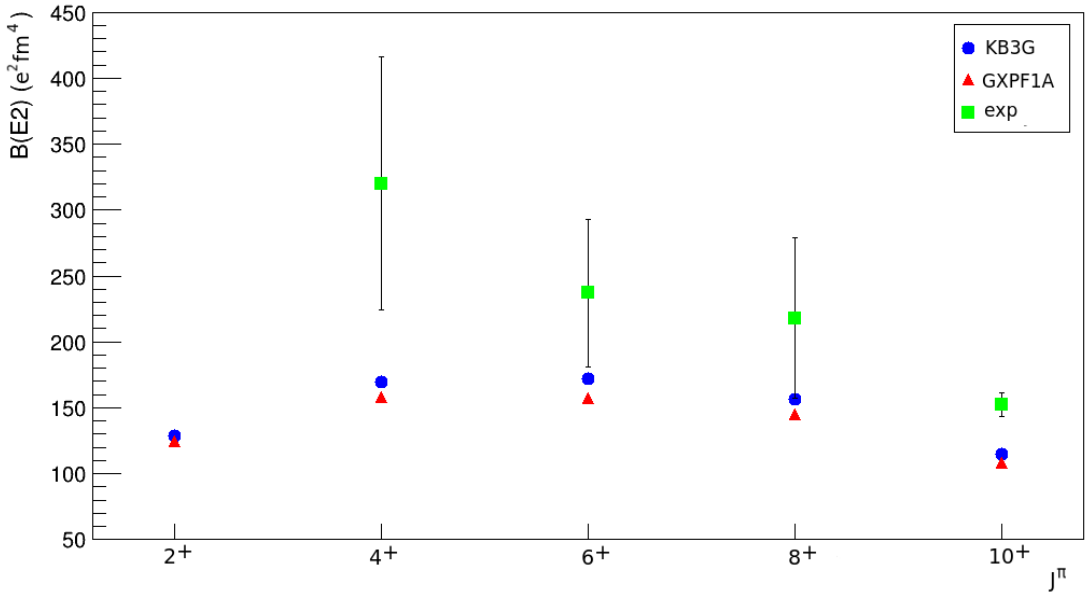

Figure 4.2: Comparison of the $B(E2, J \rightarrow J-2)$ values obtained from the experimental data and the ones from the shell model calculations for ^{46}Ti

It is important to point out that the codes used in this work for the theoretical calculations consider a closed core of the ^{40}Ca and this is a very strong assumption for the case of ^{46}Ti, only with 6 nucleons in the outer shell. This may lead to this underestimated values of the energy levels and also the transition probabilities because not all the col-

lectivity of the states may be properly reproduced without allowing cross-shell excitation across N and Z = 20.

4.2 Transition probabilities in ^{50}Cr

As in the case of ^{46}Ti the same models of interaction have been used for the theoretical calculations of ^{50}Cr. In the Figure 4.3.a it is shown a comparison of the experimental excitation energies with the calculated ones based on the KB3G and GXPF1A interactions.

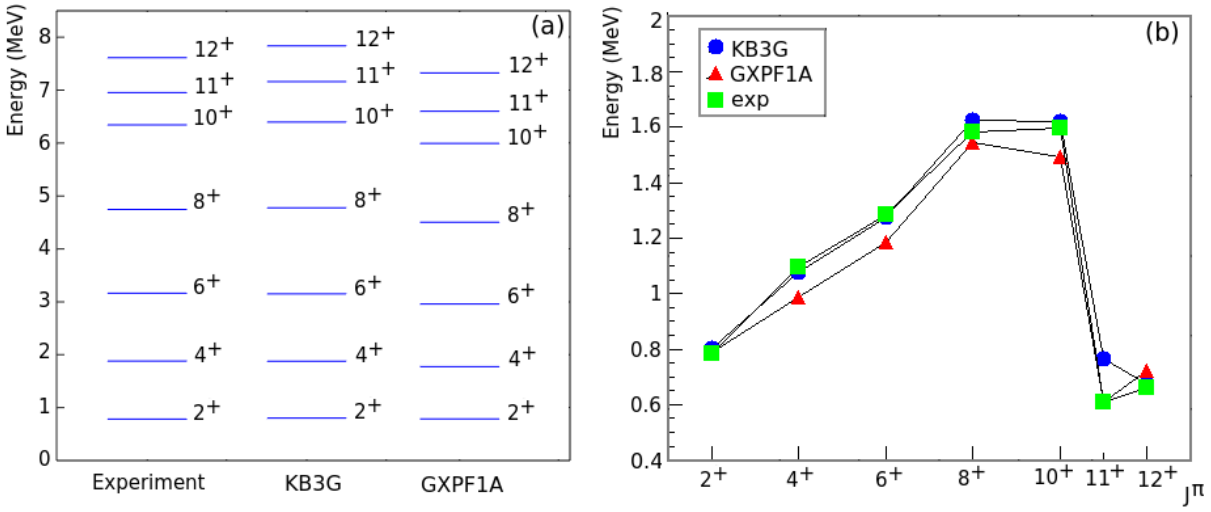

Figure 4.3: a) Comparison of the experimental excitation energies of ^{50}Cr with the calculated ones based on the KB3G and GXPF1A interactions b) Comparison of the energy of the depopulating transitions along the yrast states measured experimentally with the ones obtained from the calculations

The reproduction of the energy levels is good from both of the models especially in the low spin states. The KB3G interaction model reproduce almost the same values of the energy levels with a few keV difference from the experimental results. In the high spin states, 10^+ and above, there is a difference of about 200 keV.

In Figure 4.3.b the comparison of the energies of the gamma rays emitted from each energy level is reported. It is interesting to point out that the experimental and the calculated values follow the same trend up to the 10^+ state. The energy of the gamma-rays emitted from the states above it starts to decrease, but in 12^+ state increases again. This trend is very well reproduced from the calculations based on GXPF1A interaction. As it was described in the case of ^{46}Ti, the decrease of the gamma-ray energies emitted

from high spin states is an indicator of the changes in the nuclear structure.

There are two M1 transitions sensitive to our lifetime measurement ($12^+ \rightarrow 11^+$ and $11^+ \rightarrow 10^+$ transition, see Table 3.4). The reduced transition probabilities for the E2 transitions were obtained from the formula 4.1. The relation between the B(M1) and the lifetime of the energy level is given by:

$$B(M1) = \frac{1}{1.779 \cdot 10^{13} \cdot E_\gamma^3 \cdot \tau} \tag{4.2}$$

Where B(M1) is the reduced transition probability in μ_N^2, E_γ is the energy of the gamma released in the corresponding transition in MeV and τ is the lifetime of the initial energy level in seconds. The transition probabilities, B(E2) and B(M1) are represented below in the table 4.2 and 4.3 respectively.

Table 4.2: The reduced transition probabilities B(E2) of ^{50}Cr

Transition	E_γ (keV)	τ (ps)	B(E2) (e^2fm^4)
$10^+ \rightarrow 8^+$	1598	1.05(17)	75(12)
$8^+ \rightarrow 6^+$	1582	0.4(1)	206(52)
$6^+ \rightarrow 4^+$	1283	1.00(25)	235(59)
$4^+ \rightarrow 2^+$	1098	2.4(3)	213(27)

Table 4.3: The reduced transition probabilities B(M1) of ^{50}Cr

Transition	E_γ (keV)	τ (ps)	B(M1) (μ_N^2)
$12^+ \rightarrow 11^+$	662	0.19(7)	1.02(37)
$11^+ \rightarrow 10^+$	610	0.56(10)	0.44(8)

The comparison of the transition probabilities obtained from the experimentally estimated lifetimes and the ones obtained from the shell model calculations are shown in the Figure 4.4. The calculated transition probabilities from both the interaction models are almost the same in value and higher than the ones obtained from the experiment. The lifetime of the 4^+ state it was not possible to be measured from the DSAM method, and also it was impossible to observe higher transitions that the 12^+ state, which would complete the analysis of this band. It is interesting to point out the matching of the trend

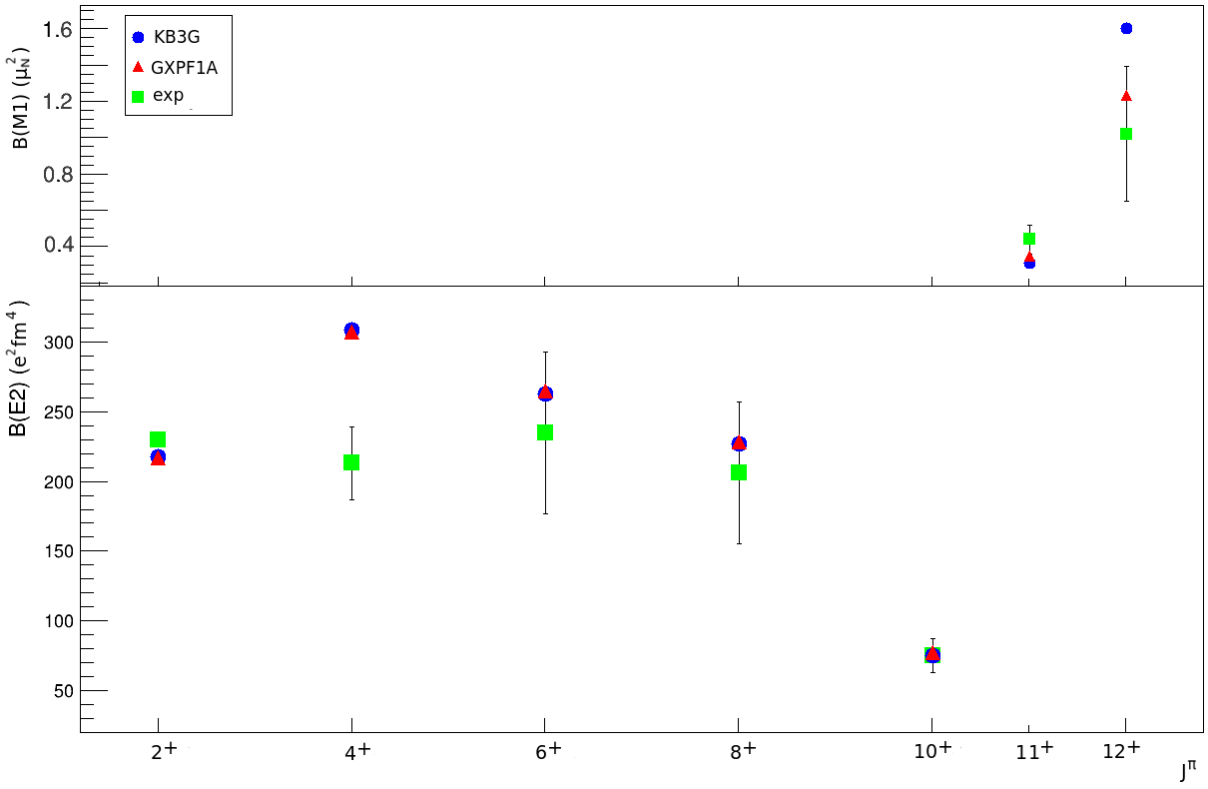

Figure 4.4: Comparison of the $B(E2, J \rightarrow J-2)$ and $B(M1, J \rightarrow J-1)$ values obtained from the experimental data and the ones from the shell model calculations for ^{50}Cr

of the experimental transition probabilities and the calculations. As spin increase above J = 4 up to J = 10 there is a decrease in the value of the transition probability, which means a transition from a collective to a single particle behaviour. In high spin states a decrease of the collectivity for this band is confirmed experimentally as expected from the theoretical calculations.

Chapter 5

Conclusions

In this thesis lifetime measurements have been performed for excited states in ^{46}Ti and ^{50}Cr using the Doppler Shift Attenuation Method (DSAM). We could study the collective behaviour of these nuclei observing the evolution of transition probabilities along their yrast line. To populate them in high spin states a fusion-evaporation reaction ^{36}Ar + ^{16}O was used. The experiment took place in Ganil (France) in 2018 using the gamma-ray tracking spectrometer AGATA coupled with two ancillary detectors NEDA + Neutron Wall and Diamant, to obtain high selectivity for the channels open in the reaction.

States up to the $J^{\pi} = 12^{+}$ have been confirmed in the case of ^{50}Cr nucleus. The lifetimes of the energy levels sensitive to our measurement method are in good agreement with the previously reported data. Shell model calculations based on two different interactions KB3G and GXPF1A reproduce properly the transition probabilities B(E2,J $\rightarrow$ J-2) and B(M1,J $\rightarrow$ J-1) extracted from the lifetime measurement. In particular the systematic trend as a function of spin expected from the calculations is experimentally confirmed. The rotational collectivity of this nucleus slightly decrease in high spin states and this has been confirmed experimentally in agreement with shell model calculations.

In the case of ^{46}Ti states up to the $J^{\pi} = 10^{+}$ have been observed. The lifetimes obtained from our experiment are shorter than previously reported measurements, however still compatible within errors. The transition probabilities B(E2,J $\rightarrow$ J-2) obtained from the shell model calculations are lower than the ones obtained from the experimental lifetimes. This disagreement may be due to the considered valence space with a closed core

of ^{40}Ca. The decrease of the B(E2) value in $10^+ \rightarrow 8^+$ transition confirms the decrease of the rotational collectivity towards the highest spin states.

Appendix A

Particle efficiency estimation

As described in Chapter 3, for the efficiency estimation the data obtained without any restriction on the trigger level have been used. A 1 proton channel has been used for the 1 proton efficiency estimation. The strongest 1p channel is the ^{47}V. For the 1 neutron efficiency estimation the ^{49}Cr channel has been chosen and for the 1 alpha channel the ^{46}Ti. More details for the gates in the gamma-gamma matrices, the peaks used for the efficiency estimation and the number of counts are reported in the figures below.

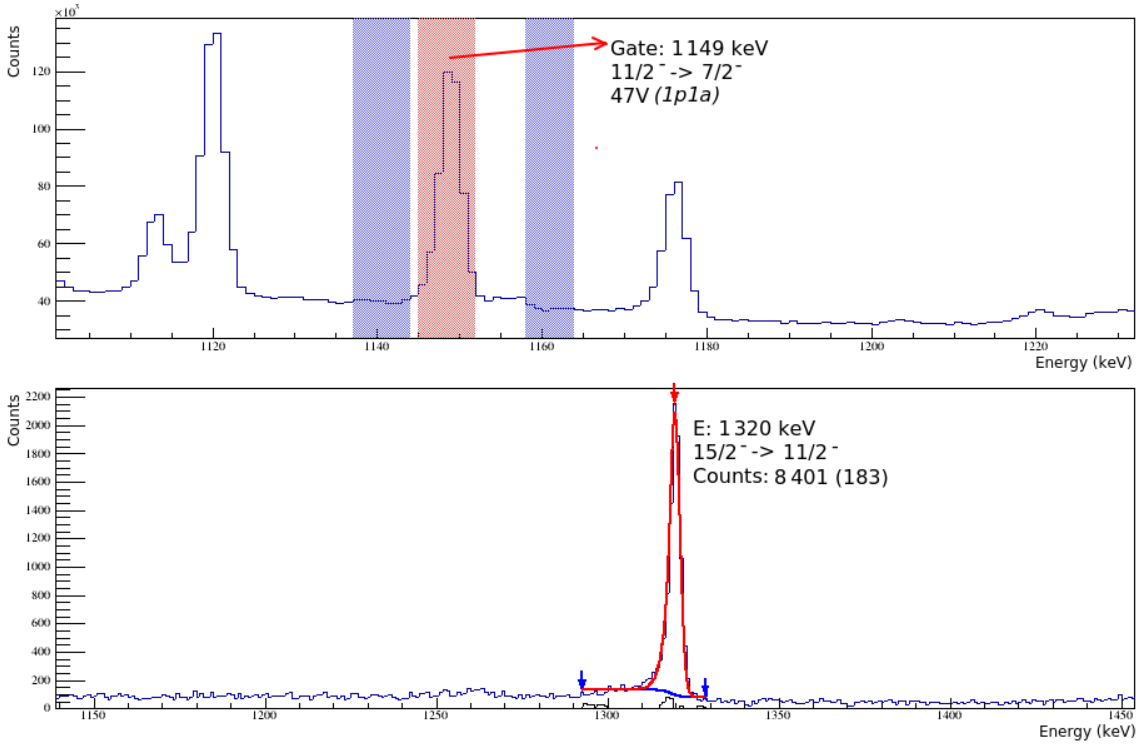

Figure A.1: The unrestricted spectrum gated on the 1149 keV ($11/2^- \rightarrow 7/2^-$) transition (^{47}V)

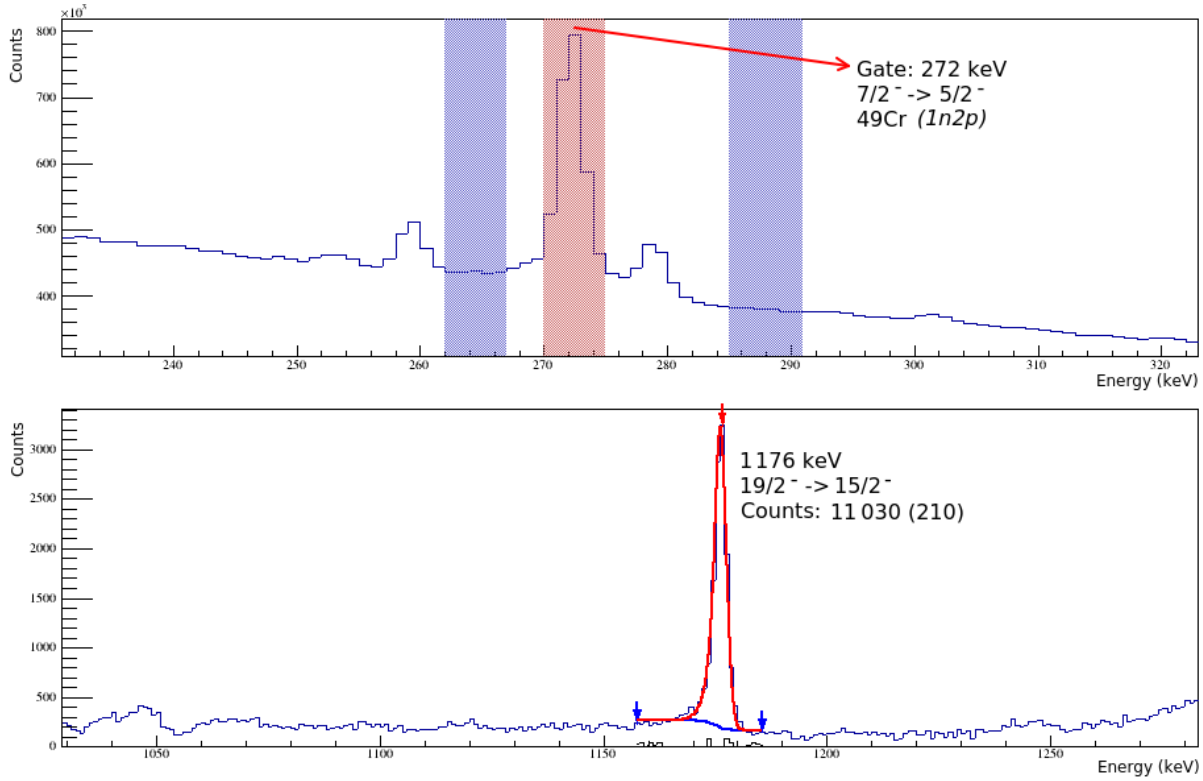

Figure A.2: The unrestricted spectrum gated on the 272 keV ($15/2^- \rightarrow 11/2^-$) transition (^{49}Cr)

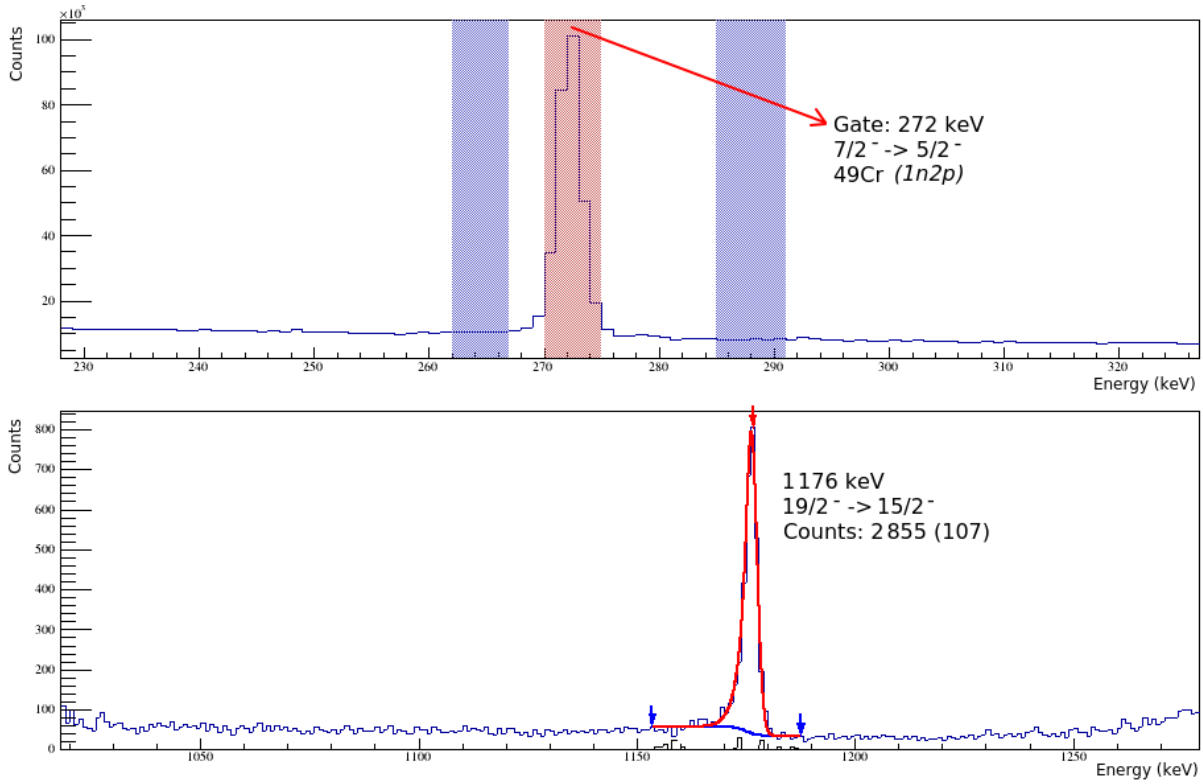

Figure A.3: The 1 neutron restricted spectrum gated on the 272 keV ($15/2^- \rightarrow 11/2^-$) transition (^{49}Cr)

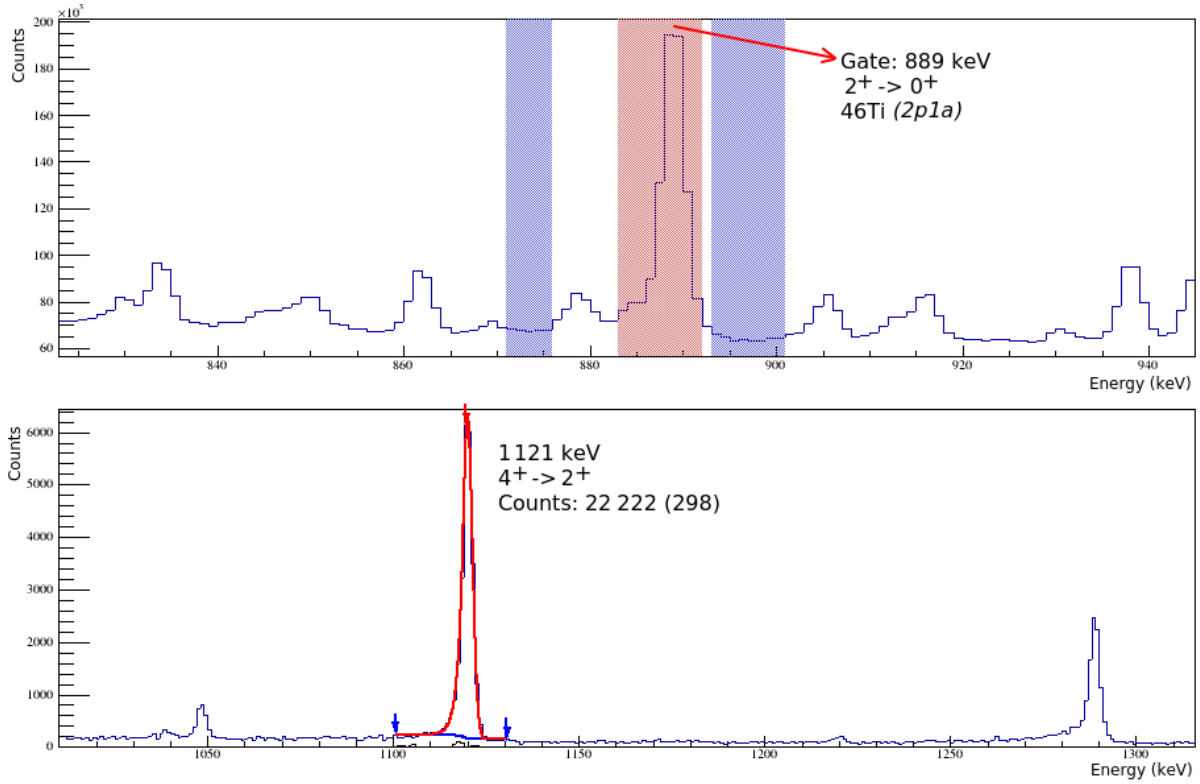

Figure A.4: The unrestricted spectrum gated on the 889 keV ($2^+ \rightarrow 0+$) transition (^{46}Ti)

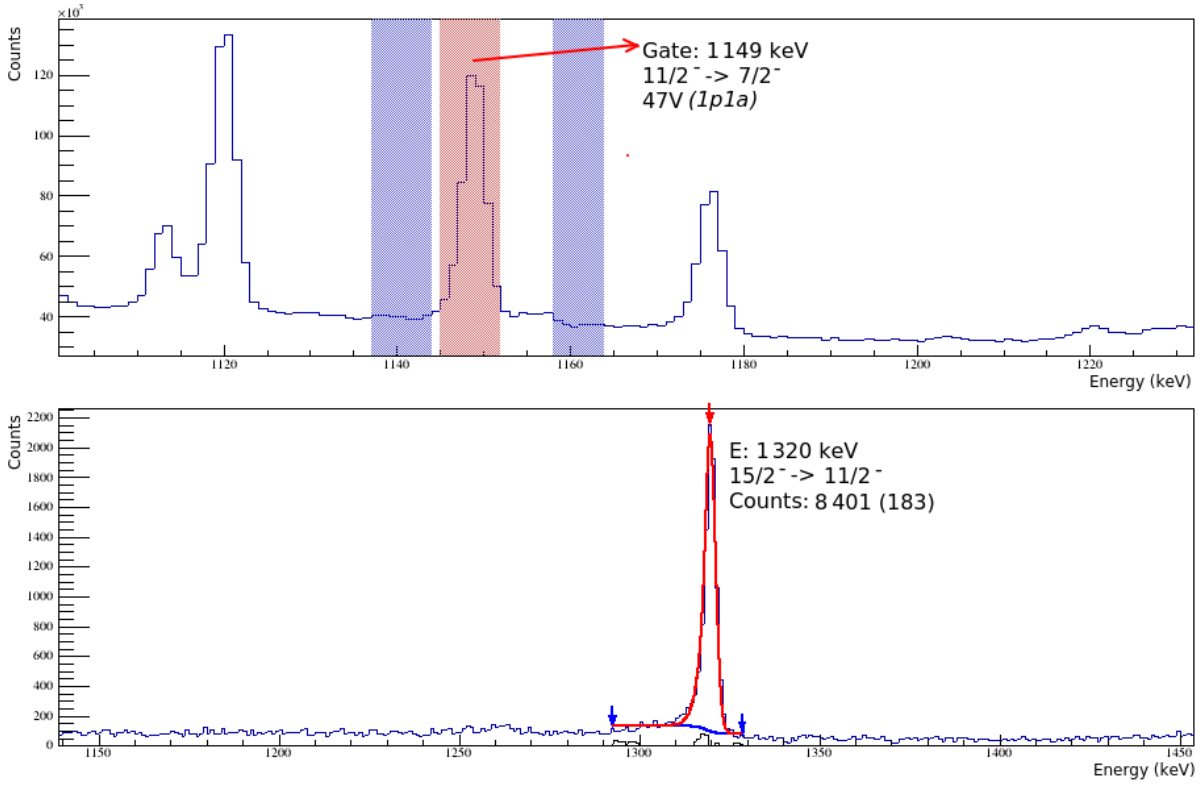

Figure A.5: The 1 alpha restricted spectrum gated on the 889 keV ($2^+ \rightarrow 0+$) transition (^{46}Ti)

Appendix B

Particle leakage estimation

As described in Chapter 3, an effective leakage value is estimated in these calculation using the total statistics obtained with the regular trigger conditions. For the leakage estimation in a 1 alpha channel, a non alpha channel has to be used. The strongest non alpha channel in our reaction is ^{49}Cr. For the leakage estimation in a 1 neutron channel ^{46}Ti channel has been chosen and for the leaking in the 1 proton channel ^{44}Ti.

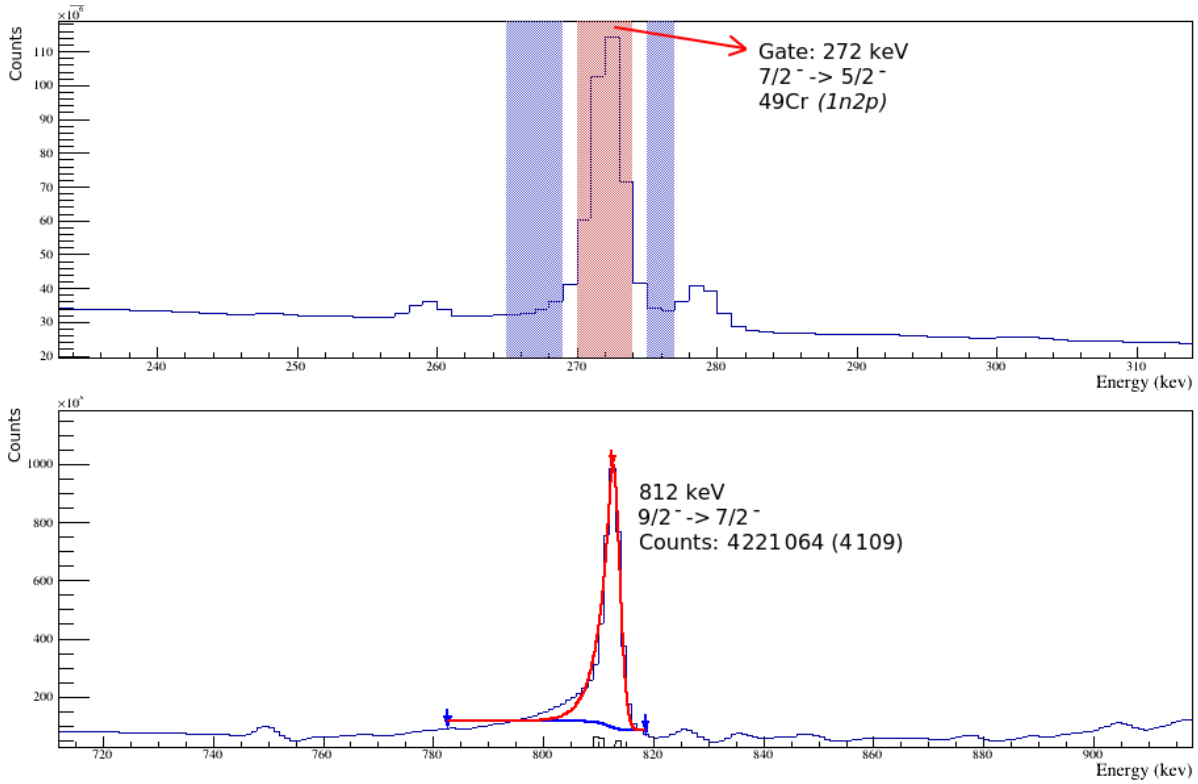

Figure B.1: The unrestricted spectrum gated on the 272 keV ($7/2^- \rightarrow 5/2-$) transition (^{49}Cr)

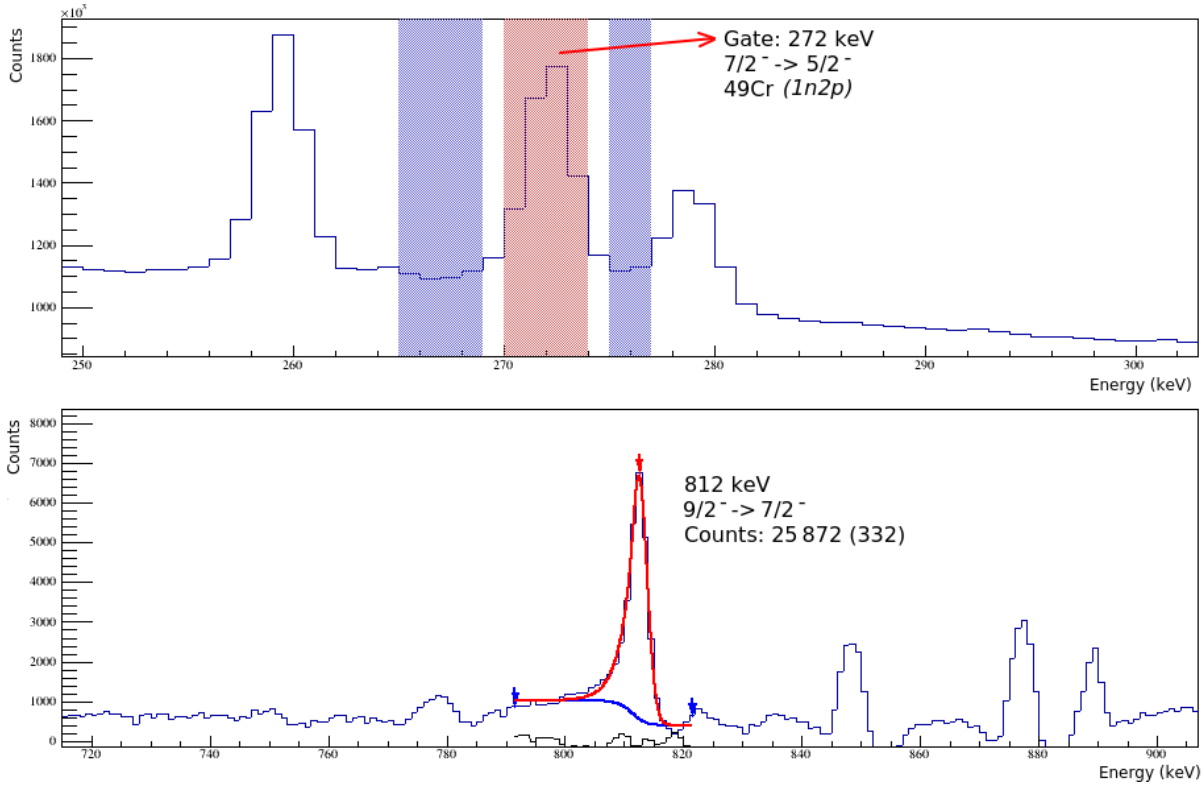

Figure B.2: The 1 alpha restricted spectrum gated on the 272 keV ($7/2^- \rightarrow 5/2-$) transition (^{49}Cr)

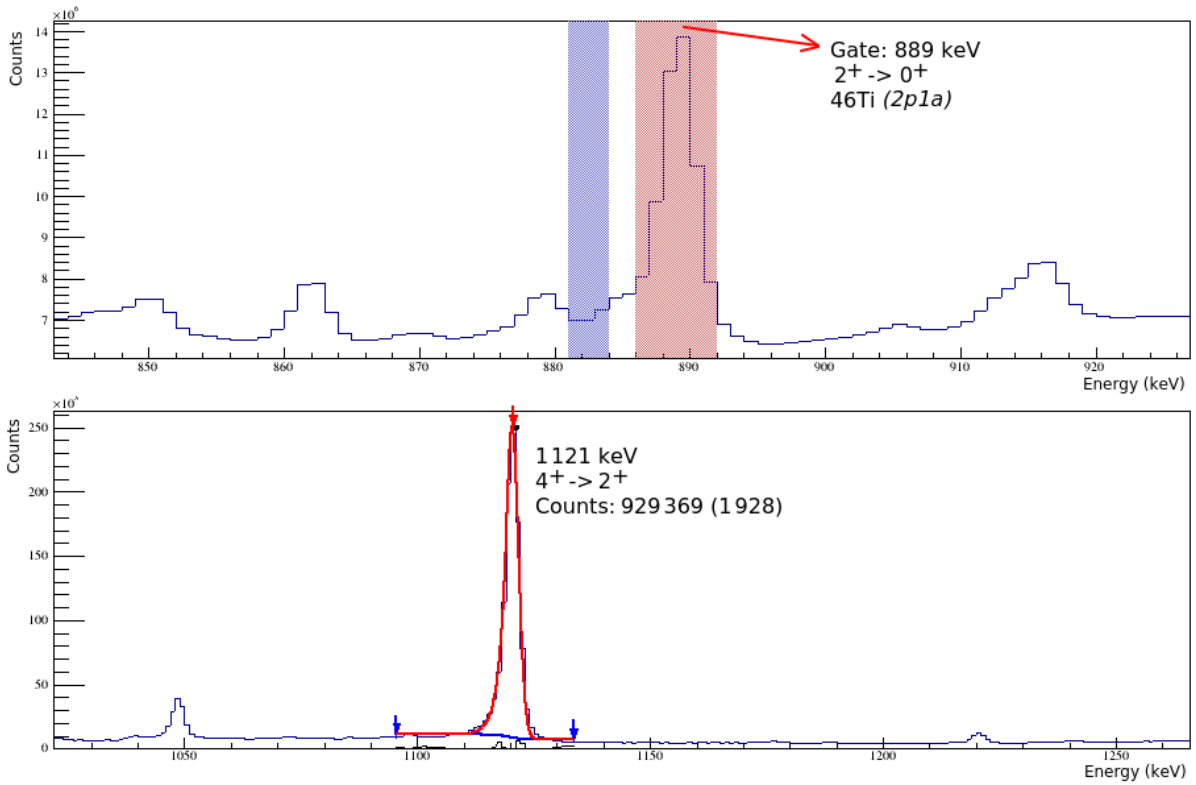

Figure B.3: The unrestricted spectrum gated on the 889 keV ($2^+ \rightarrow 0+$) transition (^{46}Ti)

Bibliography

[1] Maria Geoppert Mayer. *On Closed Shells in Nuclei.II.* Phys. Rev. 75, 1969, (1949).

[2] J. Hans D. Jensen Otto Haxel and Hans E. Suess. *On the "Magic Numbers" in Nuclear Structure.* Phys. Rev. 75, 1766, (1949).

[3] Kenneth S. Krane. *Introductory Nuclear Physics.* John Wiley, (1988).

[4] F. Brandolini and C. A. Ur. *Shell model description of $N \approx Z$ 1$f_{7/2}$ nuclei.* Phys. Rev. C 71, 054316, (2005).

[5] J. A. Cameron et al. *Spectroscopy of cross conjugate nuclei ^{46}Ti - ^{50}Cr and ^{47}V - ^{49}Cr near the $f_{7/2}$ shell band termination.* Phys. Rev. C 58, 808, (1998).

[6] G. Martınez-Pinedo. *Backbending in ^{50}Cr.* Phys. Rev. C 54, R2150, (1996).

[7] C. Alvarez. *The GASP array.* Nucl. Phys. News, 3, P. 10-13, (1993).

[8] F. Brandolini et al. *Electromagnetic transitions and structure of ^{46}Ti.* Phys. Rev. C 70, 034302, (2004).

[9] F. Brandolini et al. *Precise DSAM lifetime measurements in ^{48}Cr and ^{50}Cr as a test of large scale shell model calculations.* Nuclear Physics A, 664, P. 387-406, (1998).

[10] F. Brandolini et al. *Bands and Coulomb effects in ^{50}Cr.* Phys. Rev. C 66, 021302, (2002).

[11] D. Bucurescu et al. *Band terminations in the nucleus ^{46}Ti.* Phys. Rev. C 67, 034306, (2003).

[12] R. Ernst et al. *Shell structure of Ti and Cr nuclei from measurements of g factor and lifetimes.* Phys. Rev. C 62, 024305, (2000).

[13] F. Recchia. *In-beam test and imaging capabilities of the AGATA prototype detector.* PhD thesis, University of Padova, (2008).

[14] D. Bazzacco et al. *AGATA, Technical Proposal for an Advanced Gamma Tracking Array for the European Gamma Spectroscopy Community.* HAL, (2012).

[15] P.J Nolan. *EUROGAM: a high efficiency multidetector array for gamma-ray spectroscopy.* Endeaovur, 15, P. 22-25, (1991).

[16] F.A. Beck. *EUROBALL: Large gamma ray spectrometers through european collaborations.* Progress in Particle and Nuclear Physics, 28, P. 443-461, (1992).

[17] I-Yang Lee. *The gammasphere.* Progress in Particle and Nuclear Physics, 28, P. 473-485, (1992).

[18] C.W.Beausang. *GRETA: the gamma-ray energy-tracking array. Status of the development and physics opportunities.* Nuclear Inst. and Methods in Physics Research B, 204, P. 666-670, (2003).

[19] S. Akkoyun et al. *AGATA—Advanced GAmma Tracking Array.* Nuclear Inst. and Methods in Physics Research A, 668, P. 26-58, (2012).

[20] A. Boso. *Study of Isospin Symmetry Breaking effects in the A=23 and A=46 multiplets.* PhD thesis, University of Padova, (2019).

[21] C. Michelagnoli. *The lifetime of the 6.79 MeV state in ^{15}O as a challenge for nuclear astrophysics and -ray spectroscopy: a new DSAM measurement with the AGATA Demonstrator array.* PhD thesis, University of Padova, (2019).

[22] F. D. Vedova. *Isospin Symmetry in the sd shell: The A=31 and A=35 Mirror Nuclei.* PhD thesis, University of Padova, (2004).

[23] D. Bazin O. B. Tarasov. *LISE++: Radioactive beam production with in-flight separators.* Nuclear Inst. and Methods in Physics Research B, 266, P. 4657-4664, (2008).

[24] J.J. Valiente-Dobon et al. *NEDA-NEutron Detector Array.* Nuclear Inst. and Methods in Physics Research A, 927, P. 81-86, (2019).

[25] F. G. Moradi. *Experimental Nuclear Structure Studies in the Vicinity of the $N = Z$ Nucleus ^{100}Sn and in the Extremely Neutron Deficient ^{162}Ta Nucleus.* PhD thesis, University of Sweeden, (2014).

[26] A. Goasduff et al. *Simulations and Data Analysis of the AGATA/GALILEO HPGe array on the CloudVeneto.* INFN-LNL Report, 258, P. 243, (2019).

[27] O. Moller et al. *Transition probabilities and isospin structure in the $N \approx Z$ nucleus ^{46}V.* Phys. Rev. C 67, 011301, (2003).

[28] A. Poves et al. *Shell model study of the isobaric chains A=50, A=51 and A=52.* Nuclear Physics A, 694, P. 157-198, (2001).

[29] M. Honma et al. *Shell-model description of neutron-rich pf-shell nuclei with a new effective interaction GXPF 1.* Eur. Phys. J. A25, P. 499-502, (2005).

Acknowledgements

This work would not be possible without the help from my supervisors professor Francesco and Rafael. Thank you very much for making me feel very welcomed in the research group, for the extreme availability at any time to answer my questions and for the valuable suggestions.

Many thanks to professor Silvia Lenzi for helping me with the shell model calculations without which this work would not seem as complete.

Many thanks to professor Medina for the opinions and valuable suggestions for improving our results.

Many thanks also to all the professors from the department of Physics in the University of Seville, University of Caen, University of Padova and the coordinators of the NucPhys program. This experience it will be for sure very helpful for our carrier.

Thank you very much to all my friends for making me feel like home in these two years.

The last but not least! Thanks a lot to my family, Greta, Klodi, mami e babi, for their support.